LA-UR-18-23663
Approved for public release; distribution is unlimited.

Title: Cliff Retreat Characterization at Technical Area 54, Los Alamos National Laboratory, Los Alamos, NM

Author(s): Miller, Elizabeth D.
Birdsell, Kay Hanson
Stauffer, Philip H.
Schultz-Fellenz, Emily S.
Kelley, Richard E.
Goehring, Brent
French, Sean B.

Intended for: Report
Environmental Regulatory Document

Issued: 2020-09-30 (rev.2)

LA-UR-18-23663

Cliff Retreat Characterization at Technical Area 54, Los Alamos National Laboratory, Los Alamos, NM

Elizabeth Miller[1]
Kay Birdsell[1]
Phil Stauffer[1]
Emily Schultz-Fellenz[1]
Rick Kelley[1]
Brent Goehring[2]
Sean French[1]

[1]Los Alamos National Laboratory, Los Alamos, NM
[2]Tulane University, New Orleans, LA

April 2018

Table of Contents

Acronyms and Abbreviations

ArcGIS	Computational geographic information system software package
a.s.l.	above sea level (meters)
DEM	digital elevation model
DoD	DEM of Difference
FoS	Factor of Safety
GPS	global positioning system
LANL	Los Alamos National Laboratory
M	Magnitude
Ma	Mega-annum; million years
MDA	Material disposal area
PA/CA	performance assessment and composite analysis
PSHA	Probabilistic Seismic Hazard Analysis
TA	Technical area

1.0 Introduction

Los Alamos National Laboratory (LANL or the Laboratory) generates radioactive waste as a result of various activities. Operational waste is generated from a wide variety of Laboratory functions; environmental restoration and decontamination and decommissioned waste is generated as contaminated sites and facilities undergo cleanup or remediation. The majority of this waste is low-level radioactive waste and is disposed of at the Technical Area (TA) 54, Area G disposal facility. Area G includes Material Disposal Area (MDA) G, the portion of the facility that currently receives waste, and the Zone 4 expansion area located immediately west of MDA G. The Laboratory no longer plans to use the Zone 4 expansion area.

TA-54 is located on Mesita del Buey at the eastern margin of the Laboratory. Mesita del Buey is a relatively narrow (120 to 400m), gently sloping mesa that is lined by near-vertical cliffs. At many locations at the Laboratory, retreat along these near-vertical cliffs tends to occur in punctuated episodes marked by sizable rockfalls that are caused by the dislodgement of one or a few fracture-bounded blocks (Reneau, 1995). Fracturing around most of TA-54's perimeter, particularly the south-facing cliffs, introduces the potential for rock falls, and large, detached blocks on the canyon floor and lower cliff slopes provide evidence of relatively recent cliff failure and cliff retreat (Figure 1-1). Cliff retreat causes Mesita del Buey to narrow, posing a long-term risk to the integrity of the Area G disposal facility.

This report documents the results of a multi-year cliff retreat characterization study that was conducted to assess the potential impacts of mass wasting on the long-term performance of Area G. In this investigation, field and laboratory studies are used to (1) help establish the likely causes of cliff retreat, (2) understand past and future impacts of cliff failure, and (3) provide initial estimates of rates of cliff retreat for Mesita del Buey.

Figure 1-1. (Left) Typical appearance of the cliffs below Mesita del Buey. Note the fracture-bounded blocks on the cliff and the detached blocks on the slope. (Right) Numerous fractures are present throughout the cliff faces.

2.0 Background

LANL and the Los Alamos townsite are located on the Pajarito Plateau. The Pajarito Plateau is a high volcanic tableland that is bounded on the west by the highlands of the Jemez Mountains and bounded on the east by the Rio Grande rift (Griggs, 1964; Gardner and Goff, 1984) (Figure 2-1). The Pajarito Plateau is predominantly capped by late Tertiary to Quaternary age volcanic ash-flow tuffs of the Bandelier Tuff erupted from the Valles Caldera, located approximately 16.1 km west of Mesita del Buey. Following eruption of the Bandelier Tuff, paleotopography was eradicated, and the surface of the plateau was roughly continuous (Broxton and Reneau, 1996). The Plateau is now dissected by many narrow, steep-walled canyons that have been formed by intermittent streams. The canyons drain from west to east across the plateau, forming long, finger-like mesas between the canyons (Griggs, 1964).

TA-54 sits atop Mesita del Buey, one such "finger mesa", a relatively narrow, gently sloping mesa on the eastern margin of the Laboratory (Figure 2-2). It is bounded on the north by Cañada del Buey and on the south by Pajarito Canyon. The elevation of Mesita del Buey decreases from 2,139 m above sea level (a.s.l.) near its western end at TA-51 to 2,027 m a.s.l. at MDA G. The mesa is approximately 620 m wide at the western entrance to TA-54 (location A in Figure 2-2), narrows to 150 m (due to the formation of a small tributary on the north side of TA-54) (location B), and widens to roughly 400 m at the eastern margin (location C). At MDA G, the south-facing cliffs are deeply incised by multiple side drainages that drain into Pajarito Canyon. Conversely, the north-facing cliffs slope more gently and side drainages are not present. The cliffs at MDA G rise about 39 m from the bottom of Pajarito Canyon and about 33 m from the bottom of Cañada del Buey (Krueger, 1992).

2.1 Disposal Pits and Shafts

At MDA G, low-level radioactive waste is disposed in both pits and shafts. Construction of disposal pits began in February 1957; construction of disposal shafts began in 1965 (Rogers, 1977). The original design for low-level radioactive waste disposal at MDA G specified that "…the construction for the pits might begin near the axis of mesa and proceed toward the edge of the mesa to a minimum of [15 m] from the south cliff. By so excavating, the size and number of the joints in the rock can be observed, for joints tend to become more open near the periphery of the mesa" (Rogers, 1977). Following a survey performed by the United States Geological Survey in cooperation with the Atomic Energy Commission, additional initial requirements were that pits should be no more than 15 m deep and that open joints in the pits be sealed with fine-grained material (Rogers, 1977). The pits were also kept as far as practical from the well-defined drainage courses that dissect the mesa (Krueger, 1992; Rogers, 1977).

Figure 2-3 shows underground disposal pits and shafts as well as surface structures and buildings. The dark blue band represents a 15 m buffer and the light blue band represents a 30 m buffer around the cliff edge, where 'cliff edge' is defined as the distinct break in slope between the

shallow-dipping mesa top and steeply-dipping cliff face. Pits are generally more than 15 m from the cliff edge, but portions of several disposal units lie within 30 m of the cliff edge.

2.2 Regional Geology

Surface and near-surface geology at the Laboratory is dominated by the Bandelier Tuff (Qbt); as a result, all pits and most shafts at TA-54 have been excavated into the Bandelier Tuff (Abeele et al., 1981; Rogers, 1977; Purtymun and Kennedy, 1971). Figure 2-4 provides a stratigraphic section of the units present at TA-54 (Broxton and Reneau, 1995). The Bandelier Tuff forms the cap of most of the Pajarito Plateau and is the predominant cliff-forming unit along the canyons of the plateau, including those seen at TA-54.

The Bandelier Tuff is divided into the younger 1.26 Ma Tshirege Member (age from Phillips et al., 2007) and the older 1.61 Ma Otowi Member (age from Izett and Obradovich, 1994). The Tshirege Member consists of four cooling units; only cooling units 1 and 2 are exposed in Cañada del Buey and Pajarito Canyon along TA-54. Cooling unit 1 is a thick succession of ash-flow tuffs that was deposited over a widespread area of the Pajarito Plateau (Broxton and Reneau, 1995) and is divided into units 1g and 1v. Unit 1v is further divided into units 1v-c and 1v-u, only the latter of which is exposed at TA-54. Cooling unit 2 is also a thick succession of widespread ash-flow tuffs (Broxton and Reneau, 1995).

Information provided below about units 1v-u and 2 pertinent to the cliff retreat investigation is adapted from material found in Broxton and Reneau (1995) and Lavine et al. (2003). Units 1v-c and 1g and the older Otowi Member are not exposed at the surface in the vicinity of TA-54 and, therefore do not contribute to cliff retreat; they are not considered further.

Clarification of terminology: from a terminology standpoint, the terms *fracture* and *joint* are sometimes used interchangeably, but it should be noted that joints are actually a type of fracture. The term *fracture* describes any natural break in a geologic formation. Fractures are most commonly caused by compressional or extensional stress on a unit. Joints are fractures that are relatively planar and have little to no obvious displacement parallel to the fracture plane. Joints are typically spaced at a regular interval or angle because of the mechanical properties of a rock unit, and they generally occur as a set. Joints are commonly found in volcanic units as a result of cooling of very hot rock masses. *Faults* are fractures along which measureable displacement has occurred.

> **Unit 1v-u:** Unit 1v-u (~12-30 m thick) is a nonwelded to moderately welded, powdery white, vapor-phase altered unit. Pumice relicts typically make up 30% to 50% of the unit and are commonly up to 6 cm in diameter. Pumice accumulation zones are common near the top of this unit at TA-54; the high concentration of pumice allows the top of this unit to weather easily when water is present, causing instability in the overlying unit 2 cliffs (Broxton and Reneau, 1995). Figure 2-5 shows the typical appearance of unit 1v-u.

Unit 2: Unit 2 (~1.8-24 m thick) is a more densely welded cliff-forming unit. At TA-54, this unit is partially welded, with pumice fragments that are smaller (<2 cm) and less abundant (2% to 15%) than those observed in unit 1v-u. The base of unit 2 is commonly marked by a pumice swarm containing lapilli up to 15 cm in diameter. This unit has greater phenocryst content, mainly quartz and sanidine (Broxton and Reneau, 1995). The cliff-forming nature of unit 2 is shown in Figures 2-4 and 2-5. Unit 2 is highly fractured, with near-vertical fractures (Wohletz, 1996); these fractures likely resulted from brittle failure during the cooling contraction of the tuff after its emplacement.

The near-vertical fractures in unit 2 can be separated into (1) fractures visible from the mesa top (i.e. map view) and (2) fractures visible in the cliffs below the mesa (i.e., cross-sectional view). Fractures found on the mesa top are known as *sackungen*; these fractures propagate vertically into unit 2 and trend parallel to the cliff face (Figure 2-6). *Sackungen* introduce a zone of weakness along which episodic cliff failure and subsequent cliff retreat can occur. Fractures in the cliffs below the mesa trend at an oblique angle to the *sackungen* (Figure 2-6). Hereinafter, these fractures will be referred to as "cliff-face fractures."

Fracturing of the tuff units at TA-54 plays an instrumental role in cliff retreat along Mesita del Buey.

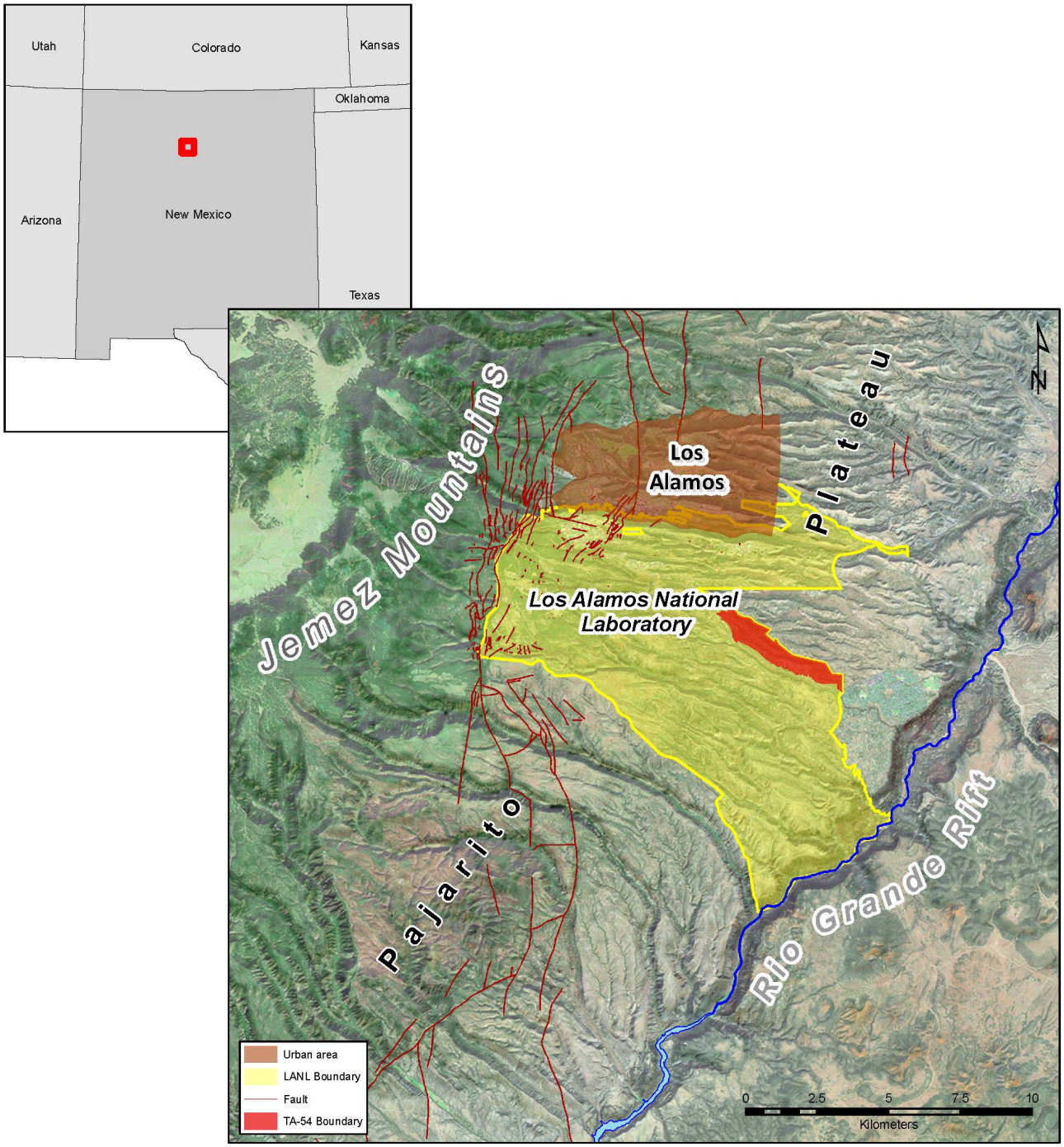

Figure 2-1. Location of Los Alamos National Laboratory, Los Alamos, NM.

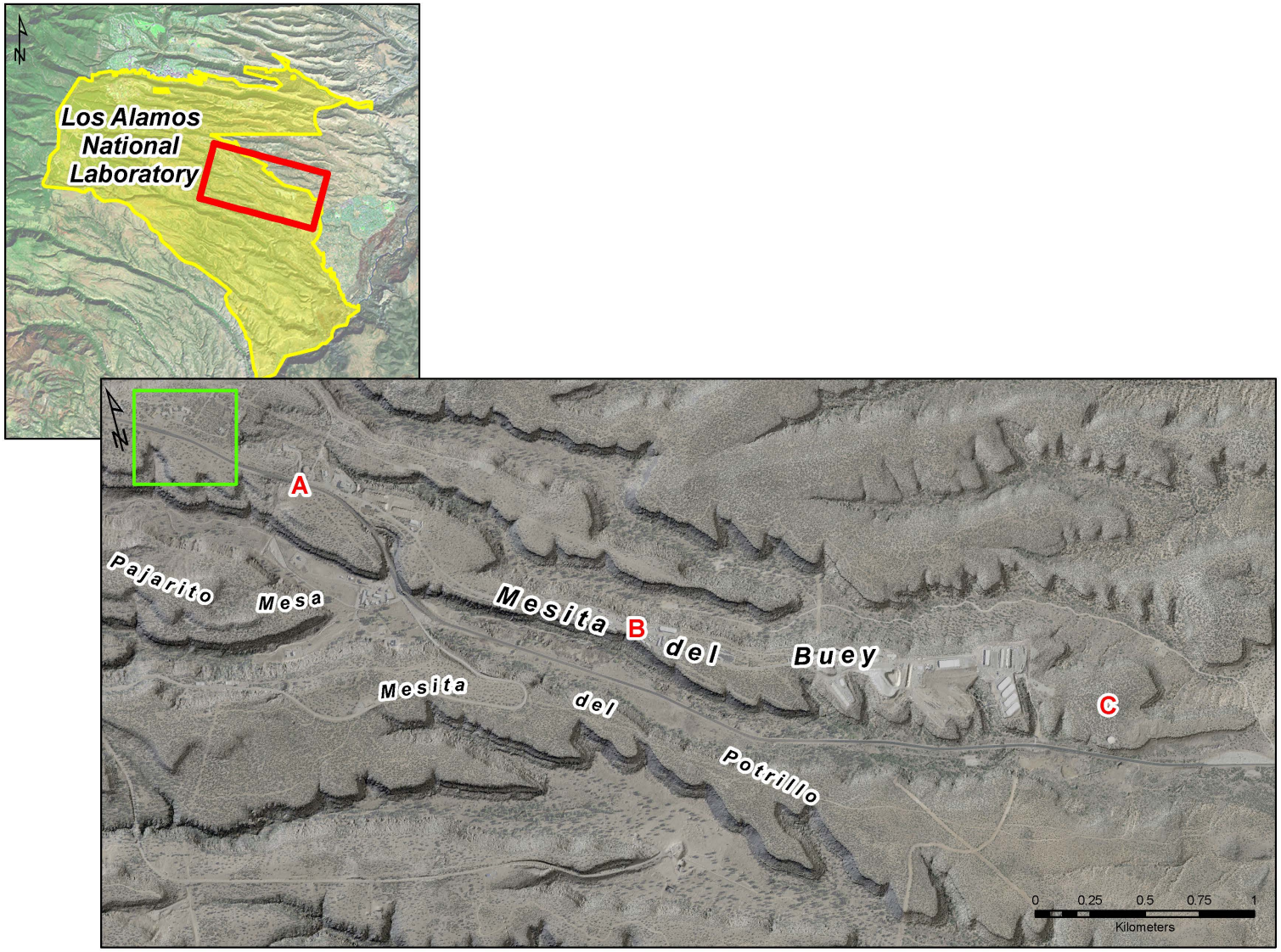

Figure 2-2. "Finger mesa" style topography that is typical of the Pajarito Plateau. The green box in the upper left of the figure is the location of TA-51 (referenced in text). Labels A, B, and C indicate the locations at which mesa width was measured.

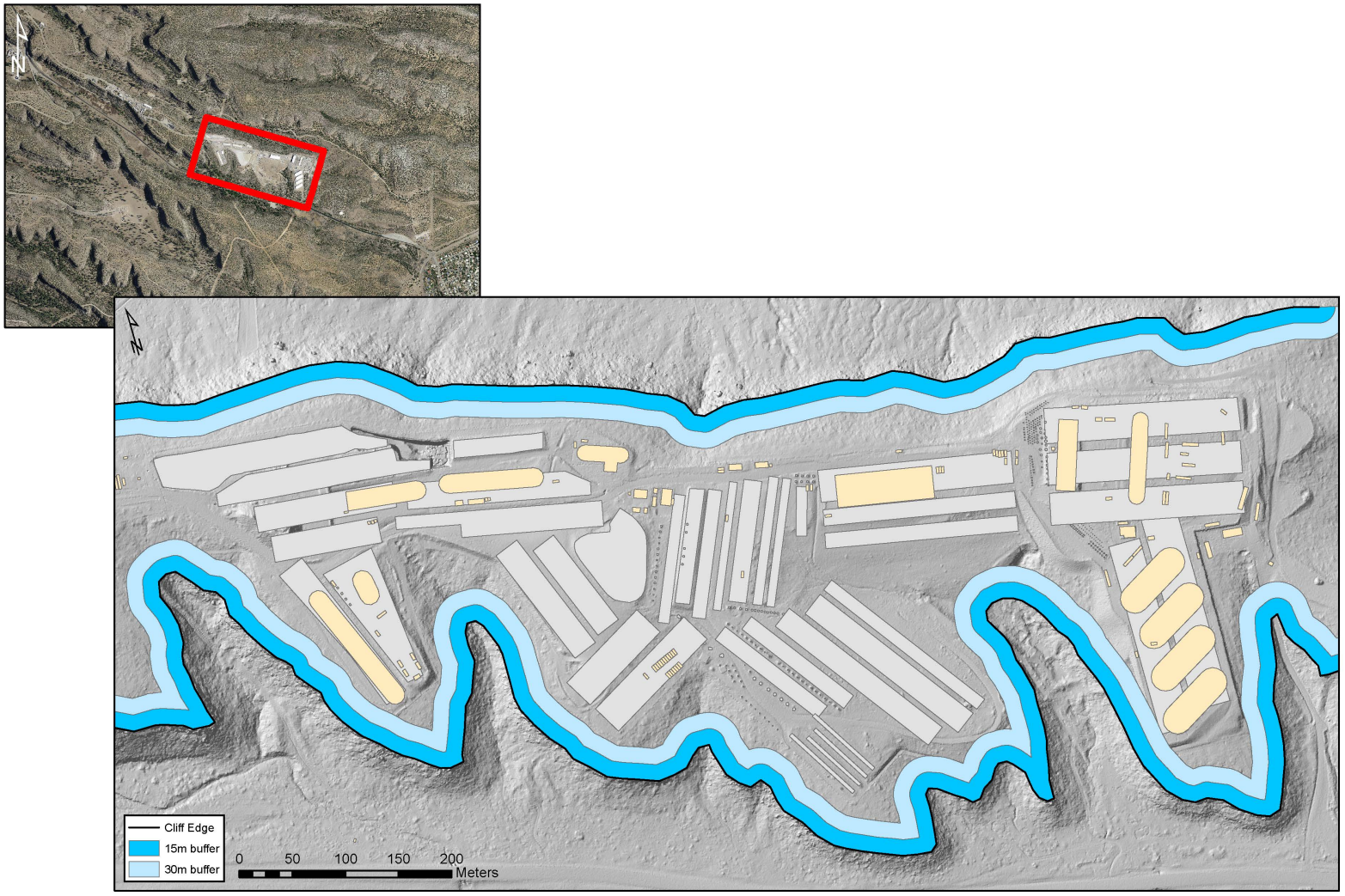

Figure 2-3. Underground disposal pits and shafts (light gray) as well as surface structures and buildings (beige). Also shown is a 15 m (dark blue) and 30 m (light blue) buffer. This buffer is calculated from the cliff edge (black), at the point where the slope breaks from mesa top to near-vertical slope.

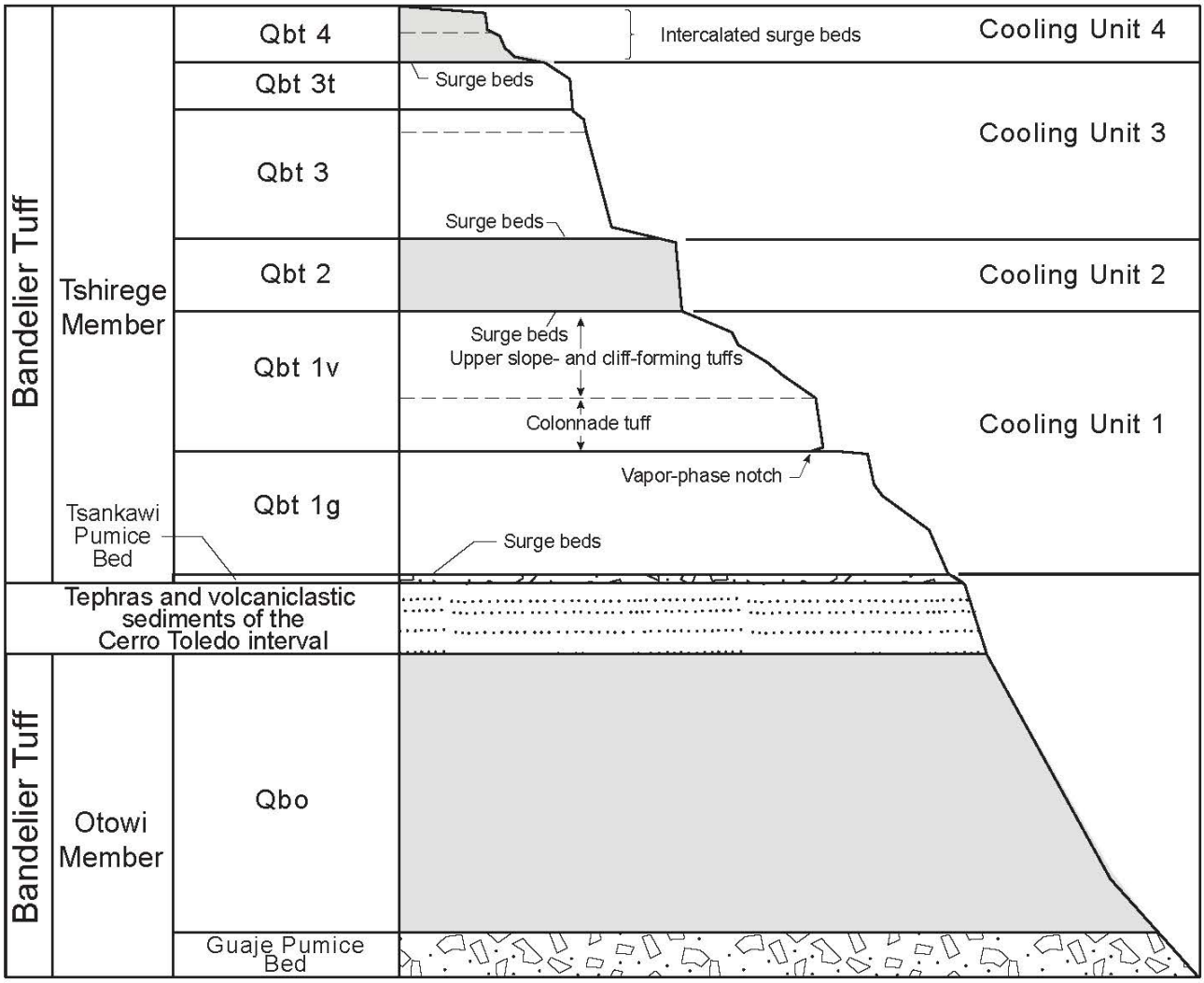

Figure 2-4. Stratigraphic cross section of the eruption of the Bandelier Tuff (Broxton and Rogers, 2007).

Figure 2-5. (Left) The less welded unit 1v-u, shown in the foreground of the image, weathers more easily. This results in shallow slope angles. (Right) Unit 2 is more densely welded and therefore forms steep, nearly vertical cliffs.

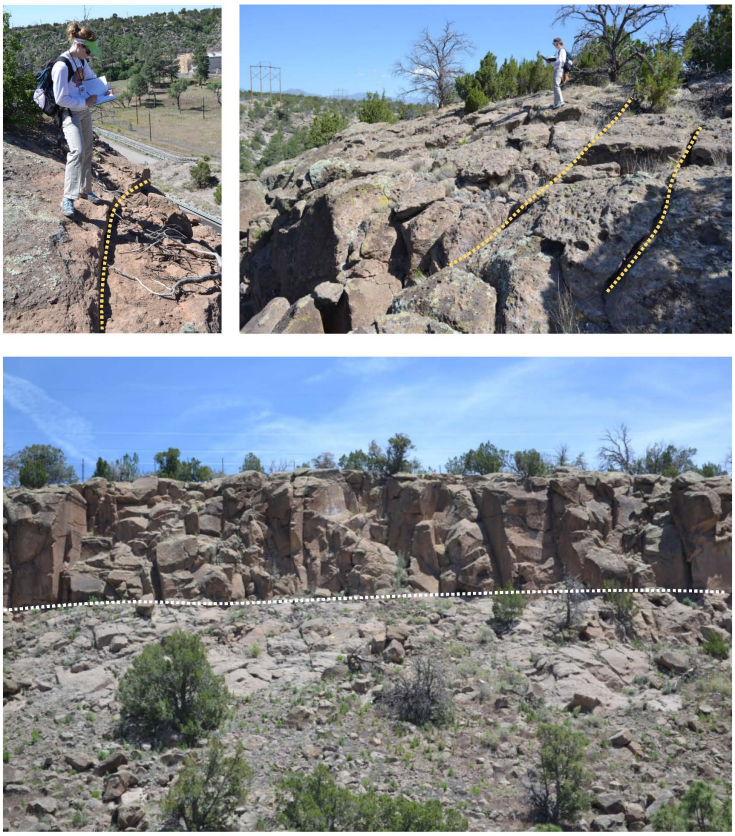

Figure 2-6. Sackungen (top) compared to cliff face fractures (bottom). The yellow dashed lines indicate sackungen on the mesa top; the white dashed line indicates the contact between the lower, slope-forming unit 1v-u and the upper cliff-forming unit 2.

3.0 Mechanisms of Cliff Retreat

Slope instability and, ultimately, failure lead to cliff retreat. Some of the factors that influence slope stability are discussed herein.

Cliff composition and configuration: The composition of the cliff-forming rocks influences the rate and pattern of cliff retreat. Poorly consolidated or highly fractured rocks tend to erode and retreat more quickly than massive outcrops of dense, minimally fractured rock. As mentioned above, unit 2 is more densely welded and maintains greater slopes for longer periods of time than underlying unit 1v-u. Differences in the degree of welding observed in units 1v-u and 2 give rise to predictable outcrop characteristics (see Figure 2-5).

Slope configuration or aspect can also lead to variations in cliff retreat rates. As discussed in subsequent sections, variations in temperature and water availability can differ greatly depending on the slope aspect, ultimately leading to variable rates of thermal forcing and freeze-thaw activity.

Cliff loading and stress: Loads or stresses placed on the cliffs may also contribute to cliff failure, e.g., slope overloading or slope modification. Slope overloading is caused when excessive building and construction on an unstable slope results in slope failure. Slope modification refers to natural or human-caused changes to the slope; causative factors include the movement of elk or deer up and down slopes and excavation by humans. For example, installation of an electrical pole near the cliff edge is believed to be the cause of a large block failure in the western portion of TA-54 (Figure 3-1). Vibrations caused by this installation likely caused the failure, and continued vibrations due to surface modifications associated with the closure of MDA G could result in additional cliff failure events.

Cliff slope and relief: The slope or gradient of the cliffs plays an important role in the stability of the rock formations surrounding the mesa (Schaetzl and Anderson, 2005). Cliffs with slopes greater than their angle of repose will be susceptible to failure and tend to topple or retreat until they reach a state of equilibrium. Cliff relief may also have an impact on stability: Rahman and Khan (1995) found high relief cliffs to be less stable than low relief cliffs with the same inclination.

Rock surface hardness: McCarroll (1991) demonstrated a correlation between rock surface hardness and rock age. Surface weathering creates a number of effects on the surface of the rocks directly related to the length of the time the rock has been exposed to the elements; surfaces exposed for long periods of time are typically softer than those exposed for short periods of time (Betts and Latta, 2000). This relationship has been used as an indirect means for estimating the age of exposed surfaces (Betts and Latta, 2000).

Extent and orientation of fractures: Generally speaking, the locations at which the exposed cliffs along MDA G fail or retreat are expected to coincide with fractures (either faults or joints) in units 1v-u and 2; these fractures represent planes of weakness along which failure can initiate or occur. S*ackungen* run parallel to the edges of the mesa; these fractures are essentially surface manifestations of toppling and flexural slip along discontinuities that dip steeply into a rock unit (Jahn, 1964; Beck, 1968). Bovis (1982) coined the term "flexural toppling" to describe this outward rotation of blocks and the dilation of *sackungen* that leads to cliff movement (i.e., retreat) over time.

Thermal forcing: Collins and Stock (2016) developed a field experiment at Yosemite National Park to study the effects of thermal forcing on rock falls. Deformation and temperature meters were installed to monitor the opening and closing of fractures at the park. Diurnal temperature fluctuations of approximately 15°C caused the instrumented fractures to expand by as much as 8 mm during the daytime; subsequent fracture closure during the cooler part of the day was not always as great as fracture opening. Over time, this thermal forcing can cause fractures to grow large enough for instability and failure to occur.

Daily temperature fluctuations are generally large at the Laboratory; June experiences an average of 14°C temperature difference between the daily high and low temperatures, while December averages a 12°C difference (Bowen, 1990). These large variations suggest that thermal forcing can play a significant role in cliff failure over time. In addition, the south-facing slopes of MDA G typically experience larger temperature gradients than the less-steep north-facing slopes, potentially leading to increased thermal failure rates.

Presence of water: The addition of water to a system with large diurnal temperature variations can contribute to freeze-thaw cycles that can damage rock. Solid ice is less dense than liquid water, thus water trapped in fractures will expand during freezing, leading to high stresses and the potential for rock fracturing. Winter temperatures at TA-54 range from about 0° to 10°C during the day and –4° to –10°C overnight. During extremely cold nights, overnight temperatures drop even lower toward White Rock and the valley (Bowen, 1990), as cold air settles into areas of lower topography. Additionally, the south side of the mesa gets direct sun for a large part of each day, amplifying diurnal temperature changes and the potential for freeze-thaw cycles.

Vegetative characteristics: Vegetation may also play an important role in cliff retreat. On the south side of TA-54, where vegetation is typically sparse, juniper and piñon trees commonly grow in fractures near the mesa edge (Figure 3-2). Over time, as new trees take root and grow, these fractures may destabilize and widen, creating a higher chance of fracture failure.

The north side of Mesita del Buey is much more densely vegetated than the south side (Figure 3-2). In part, this reflects the much different configuration of the canyon wall. Whereas a marked

difference in slope is observed between unit 1v-u and unit 2 along the south side of Mesita del Buey, the north side has a more uniform slope from the mesa edge to the canyon floor.

The reduced slopes along the north side of the mesa provide a more hospitable and soil-rich environment for plant growth; vegetation tends to grow as small grassy patches, between rocks and boulders, rather than clustering around fractures. The denser plant cover helps stabilize the cliffs along the north side of the mesa at or near the angle of repose, in contrast to conditions on the south side where plant roots penetrate into fractures.

Regional seismicity: Intense ground shaking from earthquakes may result in ground accelerations capable of fracturing rocks and causing already-fractured rocks to fail. The documented seismic activity on the Pajarito Plateau suggests that regional seismicity may play an important role in episodic cliff retreat (Figure 3-3).

3.1 Previous Cliff Retreat Studies at LANL

Several past investigations at LANL have a bearing on the occurrence and mechanisms of cliff retreat. These studies touch on fracture characteristics, seismic activity at the Laboratory, and the impacts of freeze-thaw cycling on cliff deterioration.

3.1.1 Average Erosion Rates

Previous studies have estimated cliff erosion rates both at Mesita del Buey and elsewhere on the Pajarito Plateau. Purtymun and Kennedy (1971) estimated cliff erosion rates of approximately 140 cm per 10,000 years at Mesita del Buey. Lower rates of erosion were estimated by Poths and Goff (1990), who analyzed quartz and sanidine in Bandelier Tuff for helium and neon. Cosmogenic analysis of these samples determined erosion rates to be about 18 cm per 10,000 years for more densely welded units and about 28 cm per 10,000 years for less densely welded units. Albrecht et al. (1993) used cosmic ray exposure history derived from beryllium and aluminum to estimate erosion rates for the Tshirege Member of the Bandelier Tuff; rates were found to vary from 1 cm per 10,000 years (densely welded subunits) to 11 cm per 10,000 years (less welded subunits). Using an average erosion rate based on the rates cited here, it would require nearly 4 million years to expose the waste in pits and shafts at Area G through erosion alone.

3.1.2 Fracture Studies

The nature and extent of vertical fractures in the Bandelier Tuff has been characterized in several studies. Wohletz (1996) attempted to correlate unit 2 fracture density observed along the north wall of Los Alamos Canyon with regional seismicity. A background density of approximately 20 fractures per 30 m interval was observed over an interval of 1,800 m along the canyon wall near TA-02 and TA-41. The fracture density increased to more than 50 fractures per 30 m interval in the vicinity of the TA-02 Omega West reactor building;

notable slump failure of the canyon wall is also observed in this region. The location of the reactor building coincides with a branch of the Guaje Mountain Fault, suggesting regional seismic activity and local geologic response played a role in cliff retreat and failure.

Wohletz (1996) also suggests that tectonic displacement is accommodated by preexisting fractures and therefore incrementally dispersed over a wide area. The study postulated that an increase in fracture density was attributed to the canyon walls' proximity to faults, where tectonic stresses opened new cracks along zones of weakness or incipient fractures originally caused by cooling contraction. However, field investigations by Gardner et al. (1999, 2001, 2008), and Lavine et al. (2003) did not observe surface-rupturing faults in areas where Wohletz (1996) predicted faults should be based on the increase in fracture density. It is possible faults were present in the paleotopographic setting of the Pajarito Plateau before deposition of the Bandelier Tuff, and increased fracture density in particular areas represents stress propagation through the cooling tuff above paleotopographic discontinuities.

3.1.3 ***Seismic activity***

Geologic evidence indicates that the Los Alamos area has experienced volcanic activity for the last 13 Ma (Gardner and Goff, 1984) and localized seismic activity for the last 7 Ma (Lewis et al., 2009). Some of the most recent seismic activity in the area has taken place along the Pajarito fault system, a north-northeast trending system of *en echelon* faults along the eastern flank of the Jemez Mountains (see Figure 3-3). Forming the active western margin of the Rio Grande rift near Los Alamos, the structures of the Pajarito fault system include the master, down-to-the-east Pajarito fault, and the subsidiary down-to-the-west Rendija Canyon and Guaje Mountain faults. The main Pajarito fault scarp sits approximately 8 km west of the TA-54 entrance and exhibits up to 91 m of displacement in the 1.256 Ma Bandelier Tuff west of the Laboratory's TA-16 (Lewis et al., 2009).

The Pajarito fault system provides evidence of at least one Holocene earthquake (i.e., within the last 12,000 years) of approximate magnitude (M) 7 (McCalpin, 2005); other evidence suggests as many as three more earthquakes of this magnitude may have occurred during this period (Gardner et al., 2003; Lewis et al., 2009; Schultz-Fellenz et al., in prep.). An earthquake of this magnitude would be felt over a large area and could cause considerable damage. In modern times, smaller earthquakes (M <2) have occurred north of the Los Alamos townsite along the northern portions of the main Pajarito fault (Gardner and House, 1994).

Reneau et al. (1998) identified faults, calculated structure contours on the units 1v-u/unit 2 contact and attempted to constrain the age of faulting along the southern edge of Mesita del Buey. High-precision geodetic surveying techniques were used to identify widely

distributed, small-scale faults along a traverse of the north side of Pajarito Canyon. These faults can be differentiated from fractures by offset on one or both sides of the fault. A total of 37 faults with offsets from 5 to 65 cm were recorded, most of which had down-to-the-west offsets. The fact that these faults do not rupture the surface as well as the general absence of large displacements along the unit 1v-u/unit 2 contact suggests these small displacement structures are not associated with major fault zones or systems. Reneau et al. (1998) suggested that since these faults are not clearly concentrated in discrete zones, they may record secondary deformation across the Pajarito Plateau associated with large earthquakes on the principal faults of the Pajarito fault system (several miles to the west), or perhaps earthquakes on other regional faults. The age of these small-displacement faults is not known, although the motion responsible for the faults occurred sometime within the last 1.256 Ma, after deposition of the Bandelier Tuff.

Some small-displacement faults were identified in pits at MDA G by Rogers (1977). The lateral continuity of these faults is uncertain. No surface-rupturing faults with significant lateral continuity are known to exist at TA-54 (Dethier, 1996; Goff et al., 2001; Schultz-Fellenz and Kelley, 2009).

Figure 3-1. A large block (circled in red) detached from the unit 2 cliffs during or shortly after installation of the utility pole on the mesa top.

Figure 3-2. Left: On the south side of TA-54, where vegetation is typically somewhat sparse, juniper and piñon trees commonly grow in fractures near the mesa edge. The dashed yellow line is an approximate trace of the vertical fracture in which the tree is rooted. Right: The north side of TA-54 is more heavily vegetated with less relief.

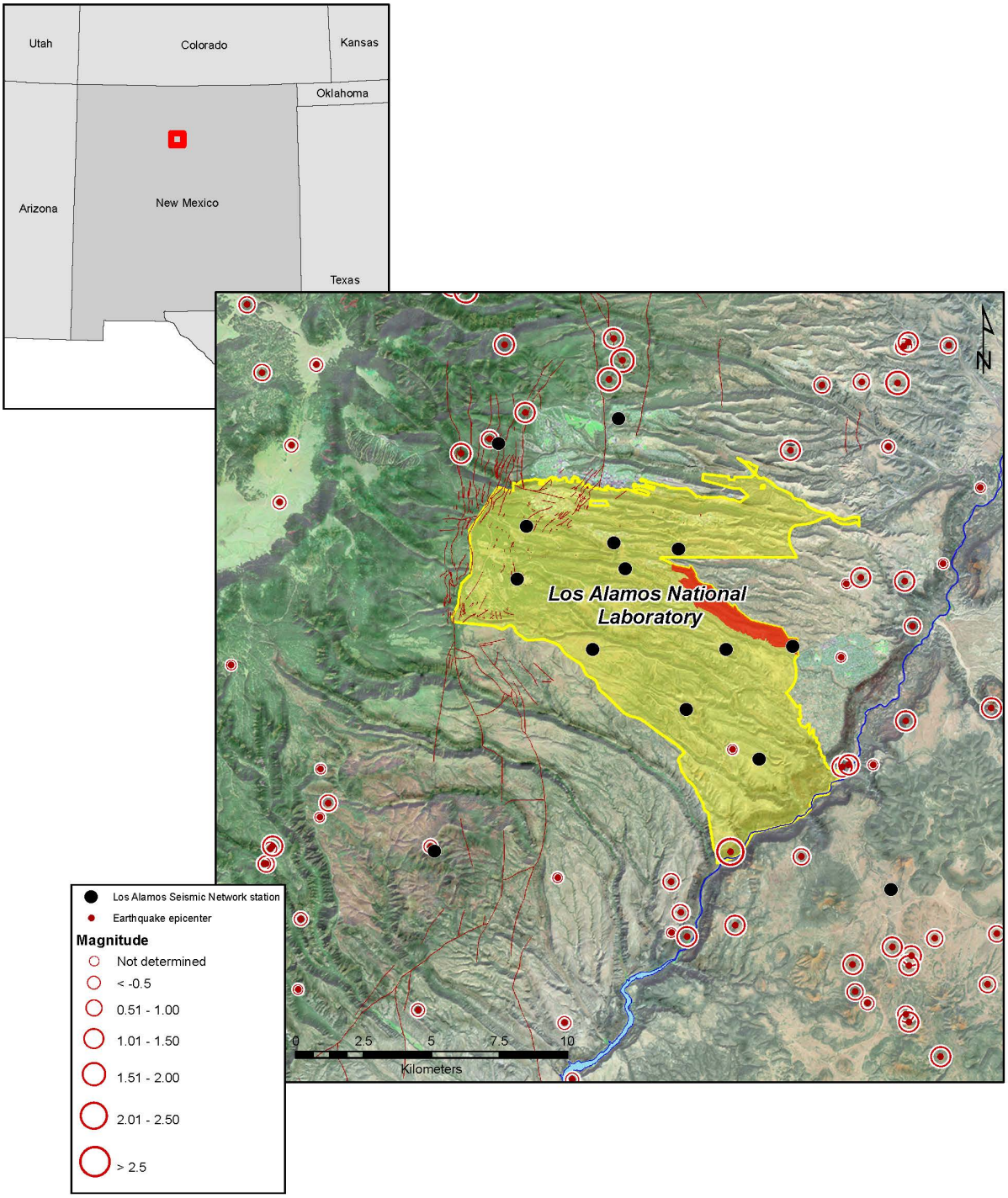

Figure 3-3. Recent seismic activity on the Pajarito Plateau (1973-2011). LANL is outlined in yellow; TA-54 is outlined in red. The western margin of LANL is demarcated by the Pajarito Fault System (brown lines).

4.0 Methods

As part of the ongoing performance assessment and composite analysis (PA/CA) investigation into MDA G, our team has performed field mapping and measurements, geographic information system (GIS) analyses, Factor of Safety calculations, and surface exposure dating investigations. These new data were collected to assess the stability of the cliffs surrounding TA-54, gain insight into likely failure mechanisms, and develop estimates of cliff retreat rates. Research was conducted over approximately six years, with a series of early investigations taking place over a three-year period (Phase I); these studies were used to inform additional studies (Phase II).

4.1 Phase I Investigations

4.1.1 Fracture Mapping and Fracture and Block Fall Characterization

Fractures found on the mesa top (i.e., *sackungen*) were mapped along the southern perimeter of MDA G using field reconnaissance techniques and ArcGIS. The perimeter was defined as the area between the fence line surrounding the disposal facility and the break in slope between the mesa top and the cliffs (Figure 4-1). The fractures were characterized in terms of their orientation, aperture, presence of fill, and, in most cases, their distance from the cliff edge. A total of 93 mesa-top fractures was mapped and characterized.

Additional *sackungen* were traced directly in ArcGIS using black and white aerial photographs of the site that were taken in 2008 and 2011. These high-resolution aerial photographs made it possible to identify *sackungen* that were not observed in the field because of a fracture's orientation (i.e., the fracture was oriented such that it was not obvious during field reconnaissance) or accessibility (e.g., some fractures were extremely close to the edge and therefore not safe to approach). Many of the mesa-top fractures are difficult to identify and trace in the field because of a lack of perspective, particularly the large-scale fractures that run the entire length of a cliff face. Using ArcGIS for a "birds-eye view" of these fractures made documentation possible.

Fractures in unit 2 that trend at an oblique angle to the *sackungen* and intersect the south-facing cliffs below MDA G (i.e. cliff-face fractures) were also mapped and characterized along the south side of MDA G; extensive colluvial cover on the north side of Mesita del Buey prohibited detailed characterization of fractures along Cañada del Buey. To conduct this characterization effort, 15 sampling zones were established on the south side of MDA G; each zone was approximately 30 m wide and oriented roughly parallel to the cliff face at the unit 1v-u/unit 2 contact (Figure 4-2). All visible fractures in the unit 2 cliff faces were measured, except for sinuous and discontinuous fractures for which it was not possible to identify a representative orientation (Figure 4-3). Figure 4-3 illustrates several

fractures that are perpendicular to the cliff face that define large blocks susceptible to failure. A total of 223 fractures were mapped along the cliff faces below MDA G.

The strike and dip of each of the *sackungen* and cliff face fractures were measured using a Brunton pocket transit compass. Fracture apertures were measured to the nearest 1 cm using a tape measure. Measurements were taken at the top, approximate midpoint, and bottom of fractures whose width varied along the length of the feature; these values were averaged to estimate a representative width. Observations on the presence of fill were also recorded.

In addition to fractures, the size of blocks detached as a result of cliff retreat were measured to gain insight into the volume of material that may be affected by cliff failure. Five of the 15 zones used for fracture characterization were selected for block fall characterization (Figure 4-2). A 30 m surveyor's tape measure was strung parallel to and approximately 1.5 m from the cliff face. Blocks that fell entirely within 1.5 m of either side of the tape measure were measured; blocks with volumes of 0.001 m^3 (measuring approximately 10 cm or less on all sides, i.e., 1000 cm^3) or less were ignored (Figure 4-4). The location of the surveyor's tape generally coincided with the break in slope between units 1 v-u and 2. The slope change between the units is sufficiently abrupt that large blocks of rock do not roll far from the point of detachment.

4.1.2 Rock Surface Hardness Measurements

Hardness values were collected to try to determine relative ages of the cliffs at TA-54; these data were supplemented with observations of cliff face color in an attempt to relate age (i.e., time of exposure) with color of the rock. All hardness measurements were conducted using a Proceq brand L-type Silver Schmidt hammer and yielded estimates of a rock's rebound coefficient, which is a measure of the rebound distance of a spring-loaded mass. The rebound distance depends upon the elastic recovery of a rock surface which, in turn, is related to the rock's hardness and compressive strength (McCarroll, 1989). Larger values of the rebound coefficient correspond to a stronger, more welded rock.

Detailed Schmidt hammer analyses were conducted at four sites within the unit 2 cliffs (Figure 4-5) that were characterized by flat rock faces exhibiting a wide range of color over a distance of 3 to 5 m. A total of 18 cliff faces were sampled: four cliff faces at sites 1, 2, and 4, and six faces at site 3. Site 1 was west of MDA G; sites 2, 3, and 4 were located within Zone 2 (cf. Section 4.1.1 and Figure 4-2). Cliff faces ranged in color from white or light tan to dark gray and lichen covered. Variations in the colors of the rock faces were discussed among field personnel and used to identify a progression from light to dark.

Three sets of 10 hardness measurements were taken on each cliff face; hardness values were then compiled in Microsoft Excel and the *trimmean* statistical analysis was applied to find the mean of the interior of the data set excluding 20% of the data points, i.e., the top and bottom outlier values. The *trimmean* function was applied to each of the three sets of ten as well as to the entire set of 30 data points.

Standard operating procedures for the Schmidt hammer recommend smoothing the rock face (using a small sander) to remove any effects of surficial deposits that may bias the rock's characterization. For this investigation, the cliff face was not sanded; Schmidt hammer measurements were taken from areas on the cliff face that were as flat and smooth as possible.

4.1.3 Photodocumentation

Two photodocumentation campaigns were undertaken 22 months apart to build a database of images of the TA-54 cliffs. These images document the current state of the cliffs and can be used for comparison to future cliff retreat characterization data.

The first photodocumentation campaign took place in June 2012. One hundred fifteen sites along the south side of MDA G were occupied to take cliff face photographs (Figure 4-6). At least one photo was taken at each site, and the compass orientation for each photo was recorded. A global positioning system (GPS) point was also collected at each location so the exact orientation for each photo could be replicated during future campaigns. Following the photodocumentation, the photos were georectified (i.e., oriented to a known coordinate system) and mosaicked using ArcGIS.

The same points were reoccupied during a second photodocumentation campaign in April 2014. This second round of photography took place 7 months after almost 18 cm of rain fell on Los Alamos County during a one-week period of near-continuous rainfall in September 2013. The photos taken during the campaign were georectified and mosaicked using ArcMap and compared with the first set of images to look for changes in the cliff face from erosion or cliff failure.

4.1.4 GIS Analyses: Slope, Topographic Relief, and Canyon Width

In 2014, airborne Lidar was collected over the entire Laboratory footprint and used to produce a digital elevation model (DEM) with 0.3 m resolution. This Lidar DEM was used for the GIS analyses described herein.

To calculate the slopes of units 1v-u and 2 around the entire perimeter of TA-54, the ArcGIS "Slope" tool was applied to the Lidar DEM. After calculating the slope, the Create Profile Graph tool in the ArcGIS toolbox extension 3D Analyst was used to create topographic profiles across Mesita del Buey (Figure 4-7).

The Lidar DEM was also used to measure canyon widths at two locations (Figure 4-8): one location in Cañada del Buey (north of MDA G) and one location in Pajarito Canyon (south of MDA G). The "Measure" tool in ArcGIS was used to quantify the canyon width as measured from the cliff edge of each finger mesa. These widths were used to estimate rates of cliff retreat at MDA G over the last 10,000 years.

4.1.5 Anthropogenic Feature Dating for Qualitative Fracture Analyses

A number of archaeological sites exist within TA-54, many of which contain rock art. It was common practice for Native Americans to use fractures in the cliff faces as boundaries for rock art (W. Bruce Masse, personal communication). Consequently, the art can be used to help constrain rates of fracturing along the cliff. To gain insight into fracture formation rates and, possibly, rates of cliff retreat, a Laboratory archaeologist was enlisted to examine several of the sites containing rock art to determine if fracturing at these sites occurred before or after installation of the rock art.

4.2 Phase II Investigations

4.2.1 Factor of Safety Calculations

Factor of Safety (FoS) is the load-bearing capacity of a structure or component. FoS is a dimensionless value that can be calculated using the simplified equation

$$FoS = \tan(\phi)/\tan(\alpha)$$

Where

ϕ = angle of internal friction
α = slope of the cliff or block face

A FoS less than one represents instability, even in the absence of external influences. Simply, the cliff is inherently unstable and will fail on its own, given sufficient time. A FoS equal to or greater than one indicates a situation in which external forces (e.g., ground motion from an earthquake) are required to initiate cliff failure (Stirling et al., 2010).

Using ArcGIS, the FoS was calculated for the TA-54 cliffs using the following ArcGIS workflow:

1. Calculate the slope of the cliffs surrounding MDA G using the 2014 aerial Lidar survey of the Laboratory and the "Slope" tool
2. Convert the Laboratory geologic map into a raster and then assign appropriate angles of internal friction to raster classes representing units 1v-u and 2. The angle of internal friction of unit 1v-u and unit 2 are 31° (Hoek et al., 1998) and 43° (Quane and Russell, 2005), respectively

3. Use the Raster Calculator to perform the FoS calculation using Equation 1

The result of these analyses indicates the cliff locations that are the least stable and therefore most likely to fail.

4.2.2 Surface Exposure Dating

Surface exposure dating, also referred to as cosmogenic nuclide dating, uses isotope concentration measurements to estimate the length of time that a rock has been exposed at or near the Earth's surface. One of the most common components of rock and sediment is quartz, which is chemically represented as SiO_2. The silicon and oxygen atoms within quartz are constantly reacting with cosmic rays (heavy particles traveling at nearly the speed of light) that penetrate into the atmosphere, mainly originating from outside our solar system; this interaction produces measurable amounts of isotopes such as Beryllium-10 and Carbon-14 that accumulate in the outer layer or "skin" of a rock face. Due to the use of beryllium at LANL and subsequent potential for sample contamination, this study used Carbon-14 cosmogenic nuclide dating.

Assuming a constant rate of production, the concentration of these isotopes in a rock's surface is proportional to the minimum length of time the surface has been exposed and experiencing cosmic ray bombardment. As a result, cosmogenic nuclide dating techniques quantify exposure dates and determine the length of time that cliff faces have been exposed; this in turn can generate a better understanding of relative cliff stability and may allow estimation of the cliff retreat rate.

Fourteen samples were collected in the fall of 2015 (Figure 4-9) for cosmogenic nuclide dating on the south side of MDA G; samples were taken exclusively from unit 2, since large rock falls are more common in this unit and pose a greater threat to the long-term stability of MDA G. Sample locations were chosen due to accessibility, lack of archaeological sites, and variety of rock face color (to analyze whether color can be indicative of approximate age). Samples were cut using a diamond-blade angle grinder to collect samples measuring roughly 30 cm by 30 cm and extending approximately 4 cm into the cliff face. Upon collection, samples were shipped to the Tulane University Cosmogenic Nuclide Laboratory for Carbon-14 cosmogenic dating analysis.

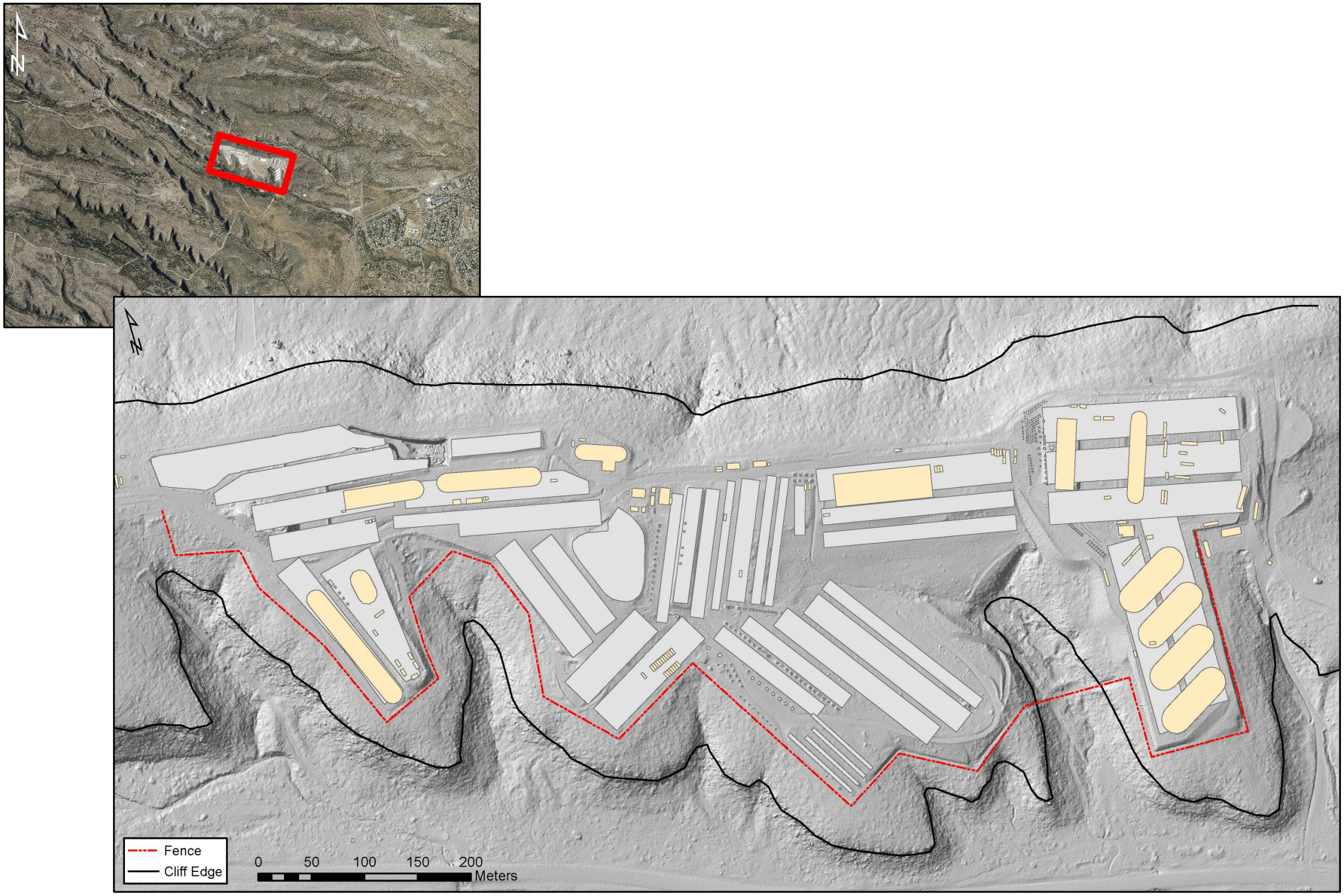

Figure 4-1. Sackungen mapping took place on the mesa top in the area between the cliff edge (black) and fence line (red).

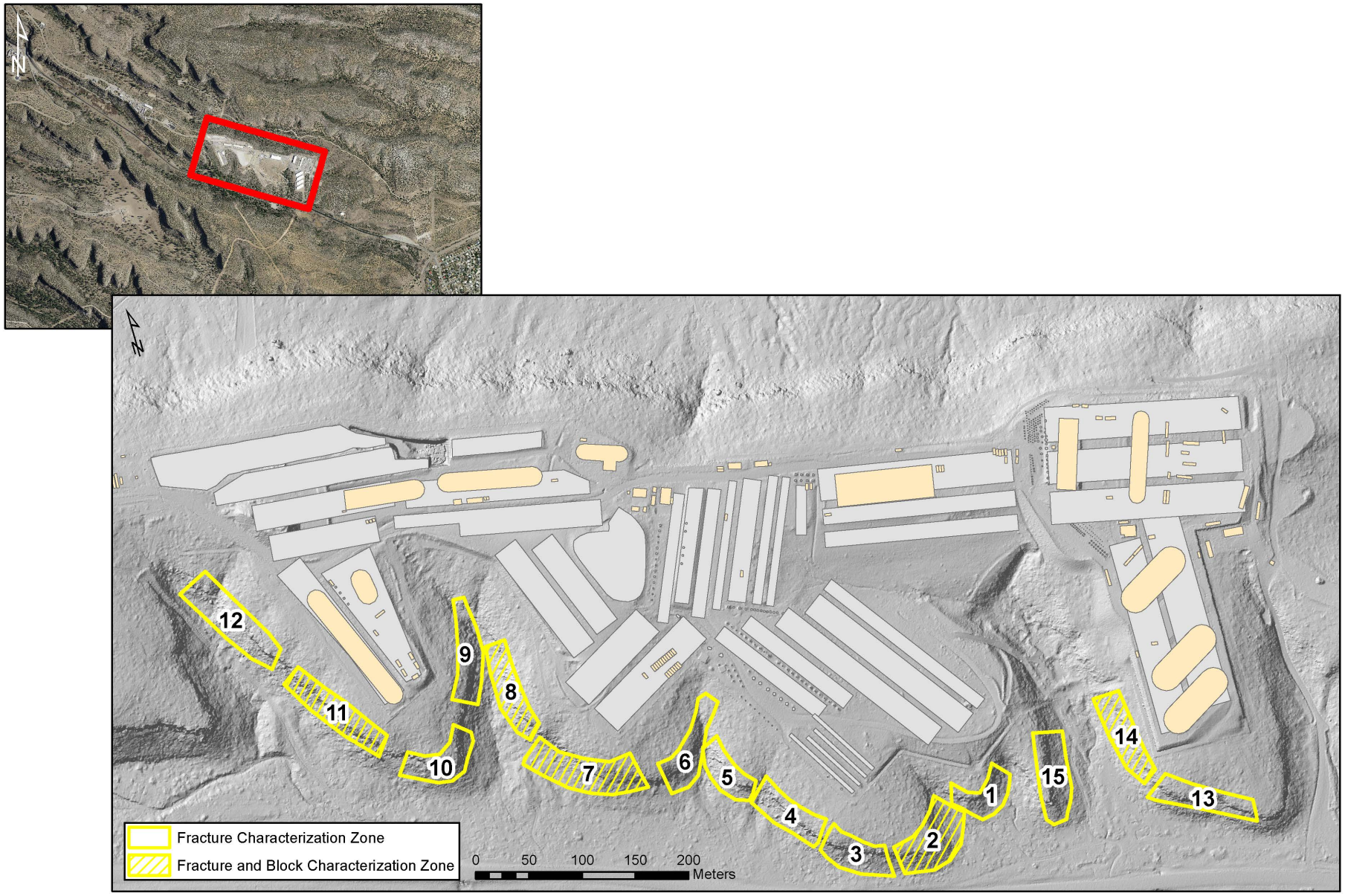

Figure 4-2. Fracture and block characterization zones on the south side of MDA G. All 15 zones were mapped for fractures; the zones with hashed lines were also used for block fall characterization.

Figure 4-3. All visible fractures in the unit 2 cliff faces were measured, except for sinuous and discontinuous fractures for which it was not possible to identify a representative orientation.

Figure 4-4. In addition to fractures, the size of blocks detached as a result of cliff retreat were measured to gain insight into the volume of material that may be affected by cliff failure.

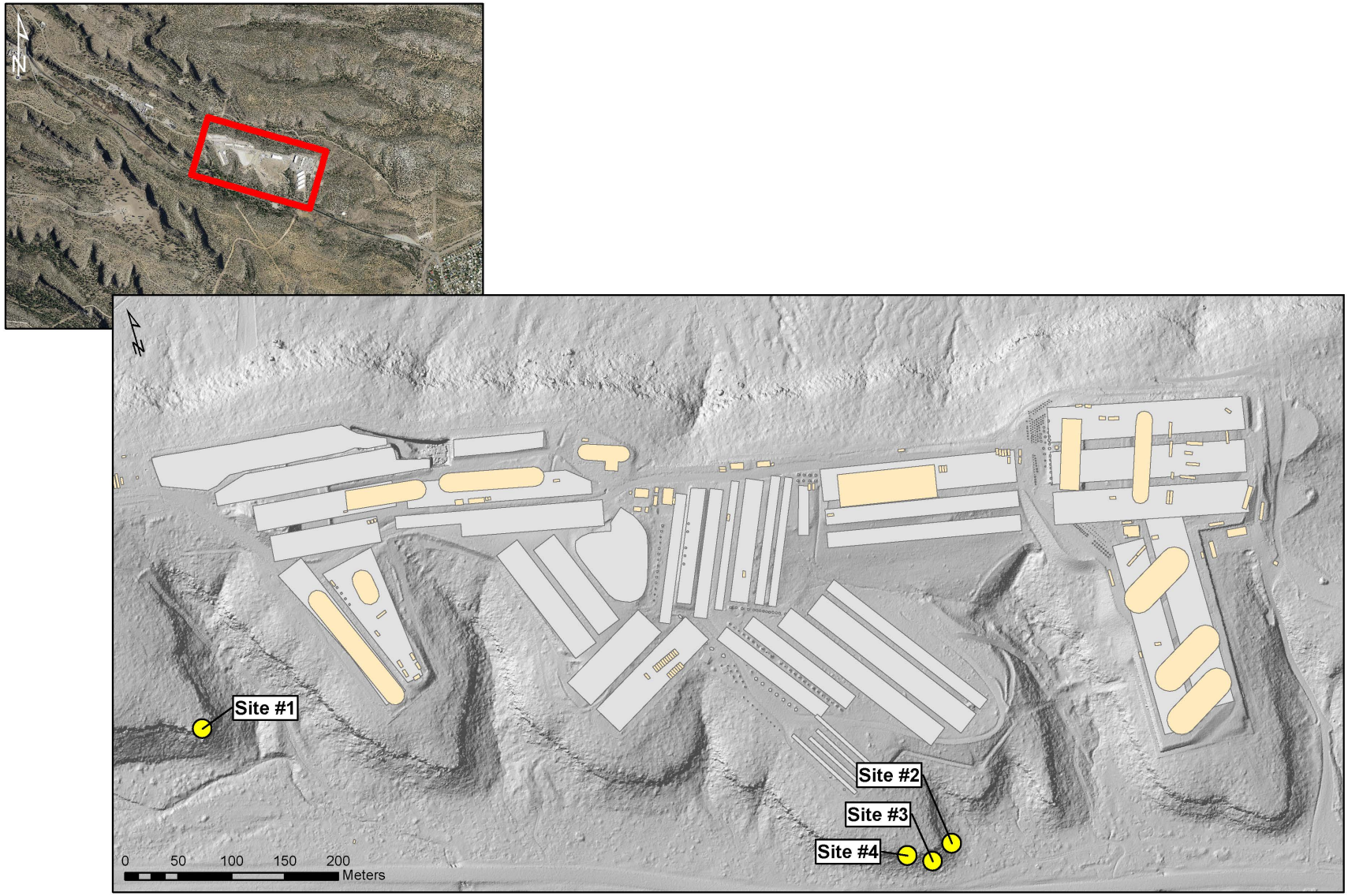

Figure 4-5. Schmidt hammer sampling locations.

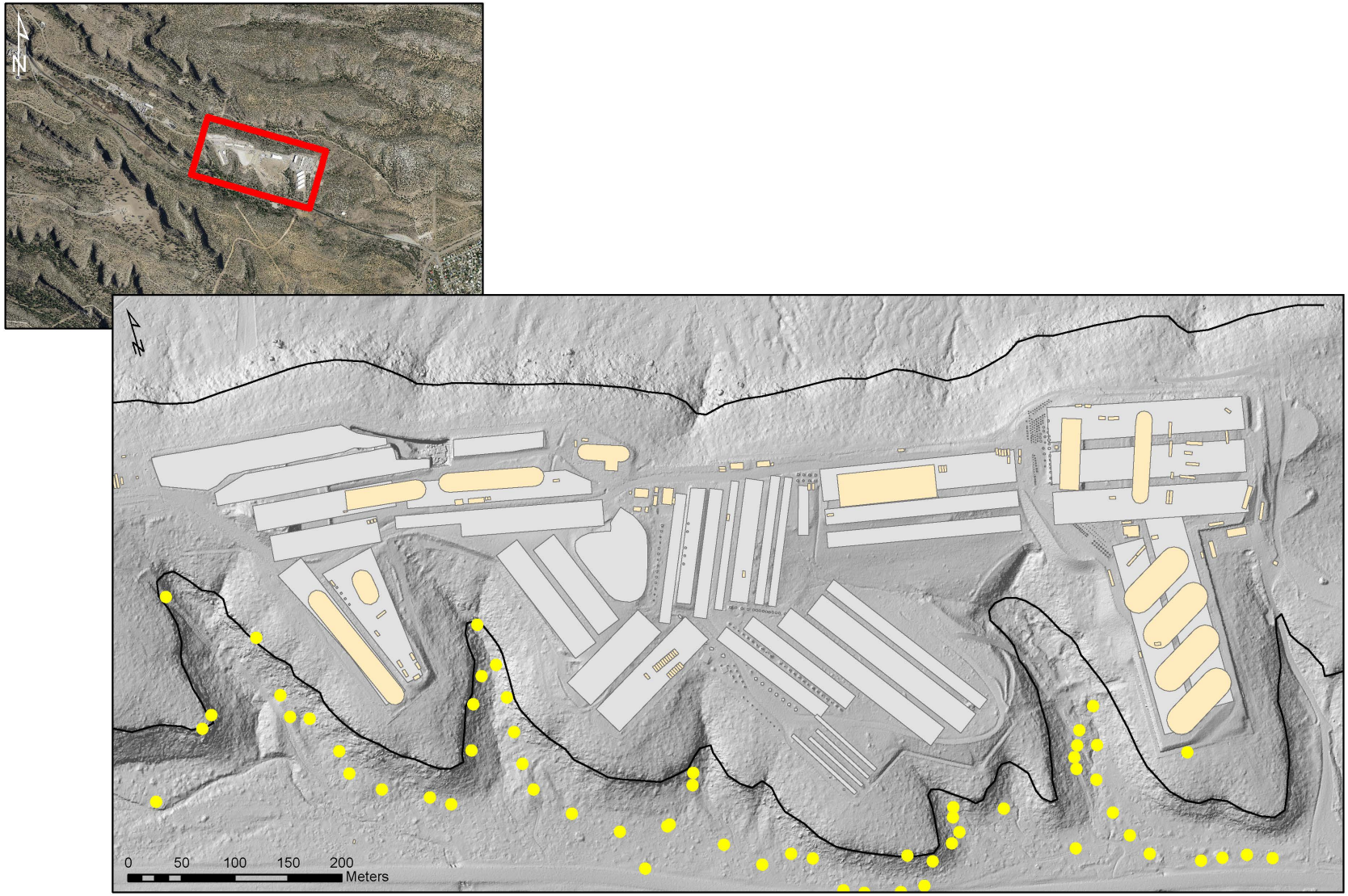

Figure 4-6. Photodocumentation locations. Each yellow dot represents a point where multiple pictures were taken to build photo mosaics of the unit 2 cliff face.

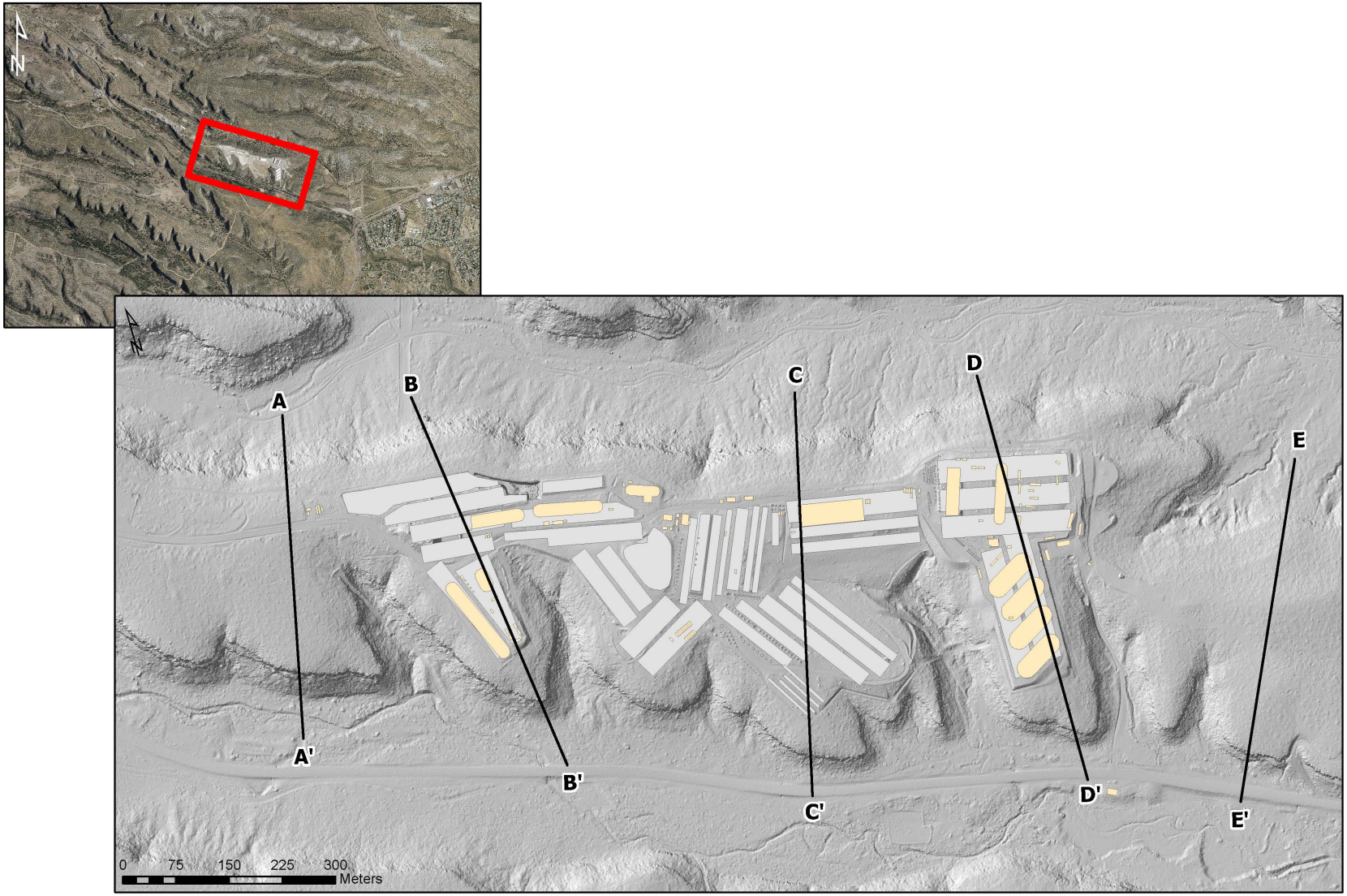

Figure 4-7. Topographic profile locations. ArcGIS was used to create topographic profiles across each of the five cross section lines.

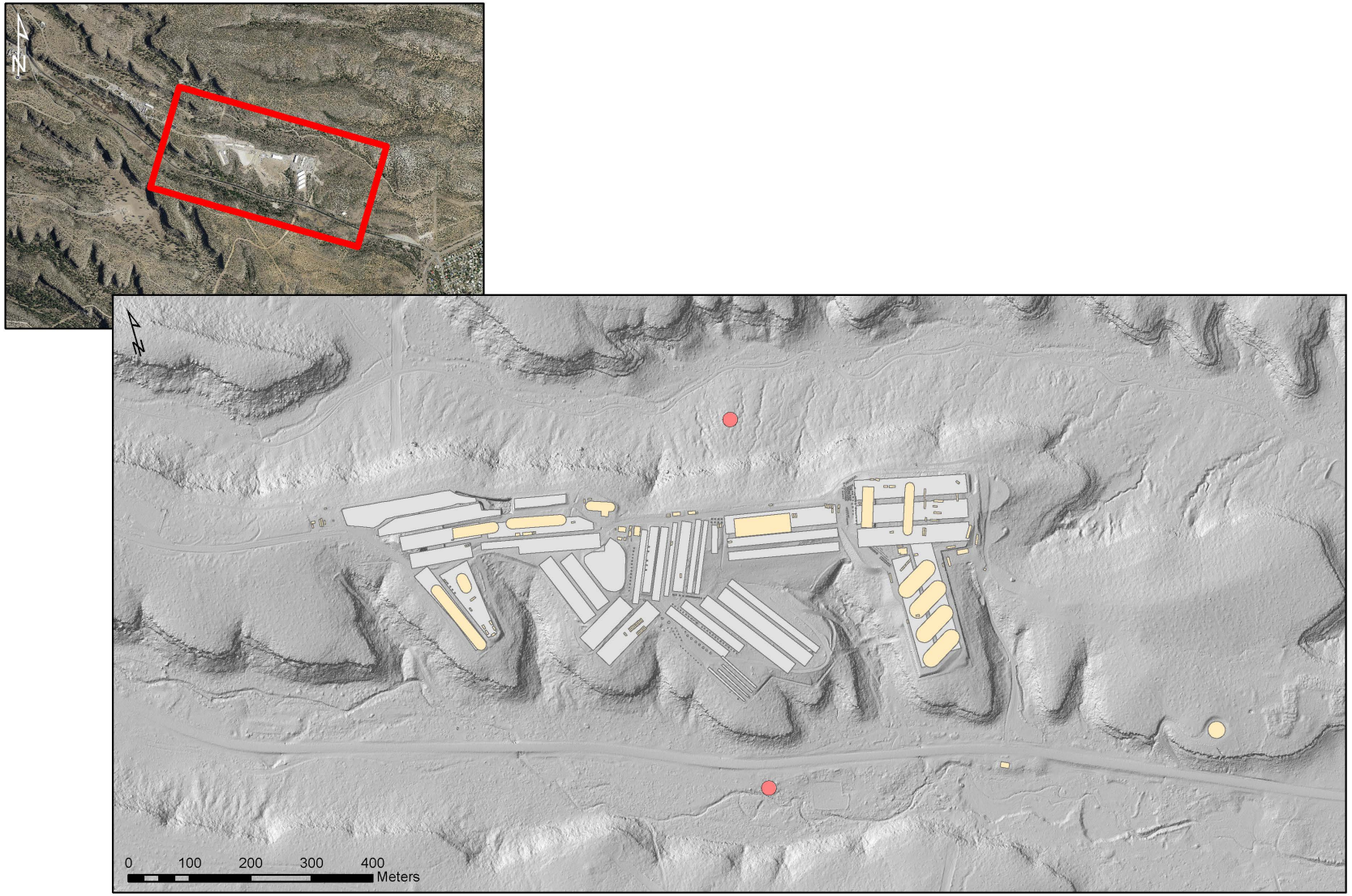

Figure 4-8. Canyon width measurement locations. Canyon width was measured perpendicular to the cliffs at the two sites indicated by pink circles.

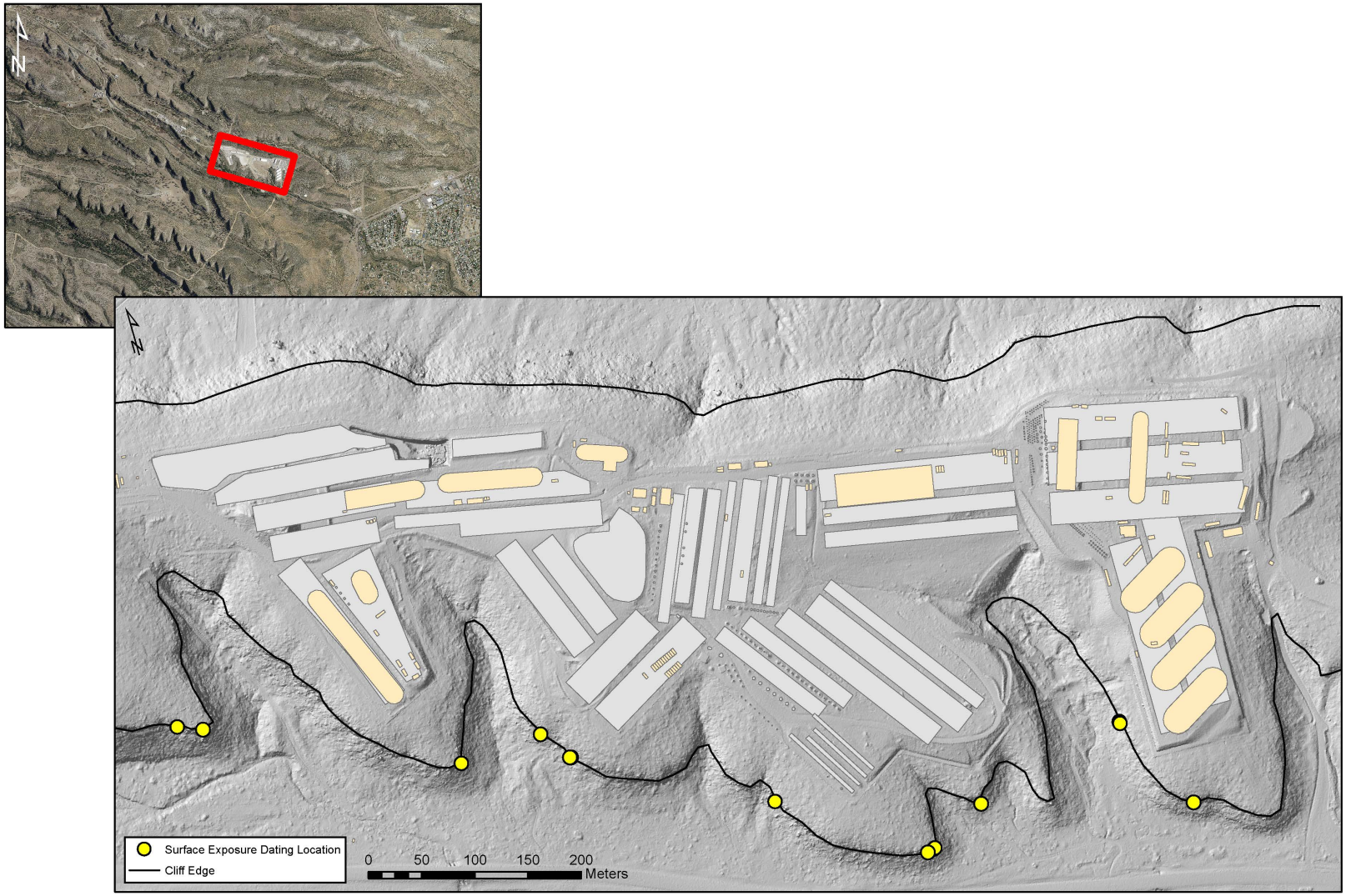

Figure 4-9. Cosmogenic dating sample locations. One sample was collected at each of the sites indicated by a yellow circle.

5.0 Results

The results of the cliff retreat characterization effort are presented below.

5.1 Fractures and Block Falls

Sackungen mapped along the south side of MDA G are depicted in Figure 5-1. The fractures shown in these plates include those identified using field measurements, 2008 and 2011 orthophotographs, and those reported by Reneau et al. (1998).

Many of the *sackungen* are oriented parallel to the cliffs below MDA G; however fractures are oriented in nearly every direction. Many of the fractures are also of significant length (10+ m). Longer fractures may indicate areas of weakness and future cliff failure. There are a few fractures that are in line with pits and shafts at MDA G, but it is not clear if any of these propagate into the disposal units. Previously mapped fractures and offsets are also included in Figure 5-1.

Field activities measured a total of 93 mesa-top fractures. Fractures were found as close as 1 m from the cliff edge and as far away as 15+ m from the cliff edge. *Sackungen* more than 15 m from the cliff edge and within the MDA G fence line were inaccessible and therefore not measured in detail. Although fractures within the fence line were not measured in the field, most of these features were captured using the orthophoto. A weathering rind separates these fractures from the cliff edge and consists of blocks of rocks that are fractured and unstable.

The distributions of apertures, fill, and dip for the *sackungen* that were mapped in the field are shown in Figure 5-2; fractures with no measurable aperture are included in the 'less than or equal to 5-cm category. The predominance of filled fractures may be a result of infilling from unconsolidated material transported with runoff following summer storms. Fracture aperture is typically greater than 5 cm; combining aperture with the steep dip of most fractures indicates that *sackungen* are near vertical planes of weakness along which failure is prone to occur.

The distribution of apertures, fill, and dip of the 223 fractures measured on the cliff faces is shown in Figure 5-3. Cliff face fractures tend to be unfilled with fracture apertures less than or equal to 5 cm. However, fracture dip remains steep.

Block fall data collected from sampling zones 2, 7, 8, 11, and 14 are summarized in Figure 5-4. Blocks have been grouped into categories based on size. The total number of failed blocks measured in the five zones and the size of the largest failed block in each zone are listed in Table 5-1.

Zone	Number of Blocks Measured	Largest Failed Block (width × height × length, m)
2	182	1.6 × 2.4 × 1.2
7	173	2.1 × 1.7 × 1.3
8	191	2.5 × 1.8 × 2.3
11	169	1.5 × 1.7 × 1.0
14	199	1.7 × 1.2 × 1.2

Table 5-1. Block Fall Measurement Data from Five Sampling Zones on the South Side of MDA G

5.2 Rock Surface Hardness

Hardness data are compiled in Figure 5-5. The data are grouped into three categories based on the color of the rock face: light, tan to gray, and varnish (Figure 5-6). The blue circles in Figure 5-5a represent the results of the *trimmean* statistical analysis for all Schmidt hammer testing on a particular face color. The orange circles in Figure 5-5b represent the results of the *trimmean* statistical analysis for each of the three rounds of Schmidt hammer testing on a particular face. Error bars on Figure 5-5a are calculated from the results in Figure 5-5b.

The shading on Figure 5-5a corresponds to the rock face colors in Figure 5-6. While the varnished rocks do have generally lower rock hardness values, there does not appear to be a direct correlation between cliff face color and rock hardness values.

5.3 Photodocumentation

Plates 1 through 8 each contain two photo mosaics: the top photo mosaic was taken during the photodocumentation campaign in 2012, and the bottom photo mosaic was taken during the 2014 campaign. Photographs were aligned as closely as possible, but time of day and lighting can make some locations difficult to detect. No plates show any indication of recent rockfalls or changes.

5.4 GIS Analyses

The cliff slopes measured at TA-54 are summarized in Figure 5-7. Areas where the slope is less than 3° have been set to null so that the background hillshade is visible. Green represents shallower slopes; red indicates steeper slopes.

The topographic profiles (Figure 5-8) illustrate the change in slope angles and relief as one travels from north to south across the mesa. The north-facing slopes experience shallower slope angles and less relief than the south-facing slopes. Additionally, as one traverses the mesa from west to east, mesa relief and overall elevation decreases.

Cañada del Buey measures 274 m wide at MDA G; Pajarito Canyon measures 210 m wide at MDA G. The canyon width measurements provide a means for estimating a long-term average cliff

retreat rate in the vicinity of Area G. The rates of retreat estimated using these measurements depend upon the assumptions made about when canyon incision began. According to Broxton and Reneau (1996), the eruption of the Otowi Member of the Bandelier Tuff largely reshaped the early Pleistocene landscape by filling in topographic lows and smoothing out the land surface, creating a broad, flat ignimbrite sheet that dipped gently to the east and southeast. Minimal erosion is believed to have occurred during the approximately 400,000 yrs that separated the eruption of the Otowi and the Tshirege Members (Broxton and Reneau, 1996). As a result, the Tshirege was erupted onto a mostly flat landscape, and there was very little, if any, pre-existing paleo-Pajarito Canyon eroded into the Otowi Member before the deposition of the Tshirege Member. Applying the assumption that erosion and canyon widening did not start until at least 400,000 yrs after eruption of the Tshirege (as was the case for the 400,000 yrs between eruption of the Otowi and the Tshirege), the maximum amount of time that Pajarito Canyon has been subject to erosion is 856,000 yrs (1.256 Ma – 400,000 yrs). This value can be used to calculate a minimum average rate of canyon widening for Cañada del Buey and Pajarito Canyon.

Cañada del Buey: The rate of canyon widening of Cañada del Buey at MDA G is given by

$$274 \text{ m}/856{,}000 \text{ yr} = 3.2\text{x}10^{-4} \text{ m/yr or } 3.2 \text{ m}/10{,}000 \text{ years}$$

The rate of cliff retreat along the southern half of Cañada del Buey (i.e. north side of Mesita del Buey) would be approximately half of this value or about 1.6 m every 10,000 years.

Pajarito Canyon: The rate at which Pajarito Canyon has widened at MDA G is given by

$$210 \text{ m}/856{,}000 \text{ yr} = 2.5\text{x}10^{-4} \text{ m/yr or } 2.5 \text{ m}/10{,}000 \text{ years}$$

The rate of cliff retreat along the northern half of Pajarito Canyon (i.e. south side of Mesita del Buey) would be half of this value or about 1.3 m every 10,000 years. Using these calculations, Mesita del Buey is narrowing by approximately 2.9 m every 10,000 years.

Applying the 856,000 yr erosion time frame to sites both down- and upstream of MDA G (Table 5-4), additional mesa narrowing calculations range from 2.6 m to 4.4 m, with an average of 3.1 m of mesa narrowing every 10,000 years.

	Downstream, supplemental sites 1 and 2				Upstream, supplemental sites 1 and 2			
	Pajarito Canyon	Cañada del Buey	Pajarito Canyon	Cañada del Buey	Pajarito Canyon	Cañada del Buey	Pajarito Canyon	Cañada del Buey
Width (m)	253	191	384	373	303	313	253	164

	Downstream, supplemental sites 1 and 2				Upstream, supplemental sites 1 and 2			
Average erosion (m/10,000 years)	2.96	2.23	4.5	4.4	3.5	3.7	2.9	1.9
Mesa narrowing (m/10,000 years)	2.6		4.4		3.6		2.4	

Table 5-4. Parameters for additional calculations of mesa narrowing estimates.

If erosion of Pajarito Canyon did not begin until more than 400,000 yrs after eruption of the Tshirege, then erosion rates and mesa narrowing would be even higher.

5.5 Anthropogenic Feature Dating

Rock art found on the cliffs that border the south side of Mesita del Buey was created during ancestral Puebloan occupation of the area and likely dates to 1300 to 1500 A.D. Fractures were commonly used as a bounding edge of the art (Figure 5-9); fractures that bisect petroglyphs may have formed after the rock art was created. A visual inspection of the rock art on the cliffs along the south side of the mesa identified sites where it was not possible to determine if the fracturing pre- or post-dates the rock art. At other locations, however, it was possible to conclude that fractures post-dated the rock art or widened since the petroglyph was created. In these cases, fracture generation or growth had occurred within the past 700 yr. An example is found near the southeastern boundary of MDA G on a sheer cliff face near the unit 1v-u/unit 2 contact that was used to create a large rock art panel (Figure 5-9). It was concluded that a secondary fracture (formed after initial cooling) that intersects the petroglyph developed after the creation of the rock art.

Another example of relatively recent deterioration of the cliff faces is seen in the south-central portion of MDA G where a distinct petroglyph is seen on a prominent rock face (Figure 5-9). Although only the top half of the figure can be seen, visual examination of the site led to the conclusion that the lower half of the petroglyph had been eroded away, likely either by fast-flowing water during monsoon seasons or dislodgement by freeze-thaw action. This erosion likely occurred within the last 500 to 700 years, after the creation of the rock art.

5.6 Factor of Safety Evaluation

Results of the FoS calculations in ArcGIS are shown in Figure 5-10. Any locations with FoS values greater than 1 are stable and therefore have been removed from the figure. The result is a figure that shows the FoS values that are less than 1; red indicates very low FoS values (and therefore

very unstable locations) and blue indicates values approaching 1 (still unstable but approaching equilibrium).

Upon comparison of the slope map and the FoS figure, it is obvious that the locations with higher slope result in a lower FoS value and therefore are less stable. While this result is to be expected, the FoS calculations serve to highlight the cliff locations with the lowest FoS values and therefore the least stable and highest likelihood of future failure.

5.7 Surface Exposure Dating

Results of the surface exposure analyses are shown in Figure 5-11 and Table 5-5. Blue circles represent the youngest exposure dates (0-2,500 years), orange circles represent exposure dates of 2,501 to 5,000 years, purple circles represent exposure dates of 5,001 to 10,000 years, and green circles represent the oldest exposure dates (10,001+ years). The youngest exposure date is 1,886 years and the oldest is 12,542 years.

Erosion rates can be estimated using the surface exposure dates (Table 5-4). Erosion rates are calculated as maximum limiting erosion rates under the assumption that the cliffs are accumulating cosmogenic nuclides at steady state with respect to the half-life of Carbon-14 and the erosion of the sample surface. The concentration (N) of a sample is described using the following equation:

$$N = \frac{P^{14}}{I^{14} + (E \times \rho \div L_{sp})}$$

where P^{14} is the production rate for a given sample, I^{14} is the Carbon-14 decay constant, E is the erosion rate in cm/yr, ρ is the sample density, and L_{sp} is the spallation attenuation length (160 g/cm^2). Surface exposure dating results show that cliff retreat has actively occurred within the last 10,000 years.

Sample	Age (yrs)	Sample description	Erosion rate (cm/10,000 yrs)
1	3305 ± 68	No shielding; soft and easy to cut	210.5
2	12535 ± 408	Shielded side canyon; eroded and toppled boulders	27.6
3	12542 ± 407		27.7
4	8802 ± 221	Minimal shielding; competent rock. Sample taken from a block that had toppled from the cliff	46.2
5	2391 ± 50	South-facing, minimal to no shielding; poorly welded, crumbling sample	282
8	3992 ± 81	Minimal shielding; soft and easy to cut	155.5

Sample	Age (yrs)	Sample description	Erosion rate (cm/1000 years)
10	10633 ± 301	Some lichen growth and the appearance of more weathering with a higher occurrence of boulders and fresh surfaces	34.7
12	4267 ± 87	Shielded, near side drainage; difficult to cut and sample	145.5
14	1886 ± 42	Minimal shielding; soft and easy to cut	374.7

Table 5-5. Surface exposure dating age results, 1σ uncertainty, sample location and rock description, and erosion rates. See Figure 5-12 for pictures of each sampling location.

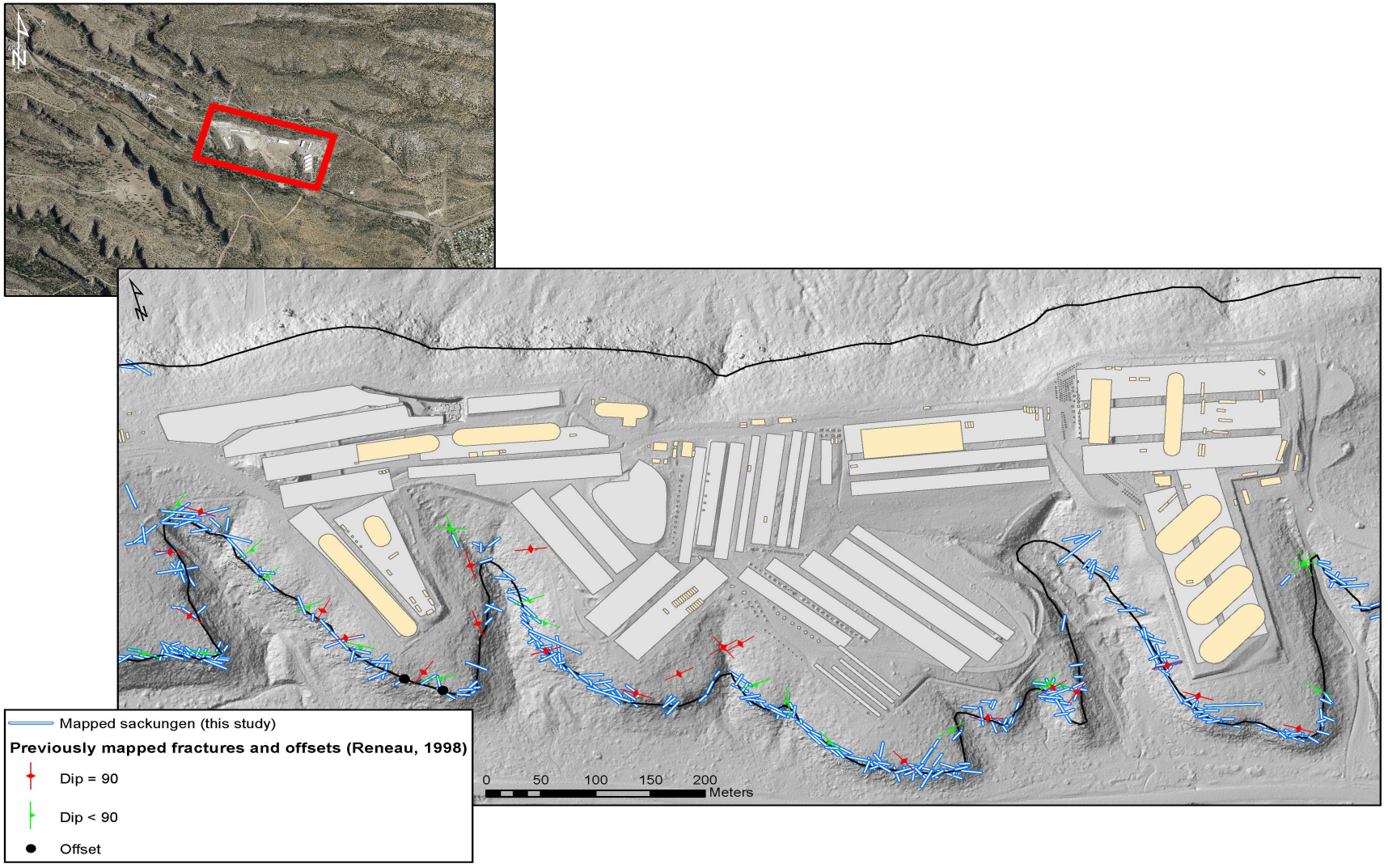

Figure 5-1. Mapping of sackungen on the mesa top.

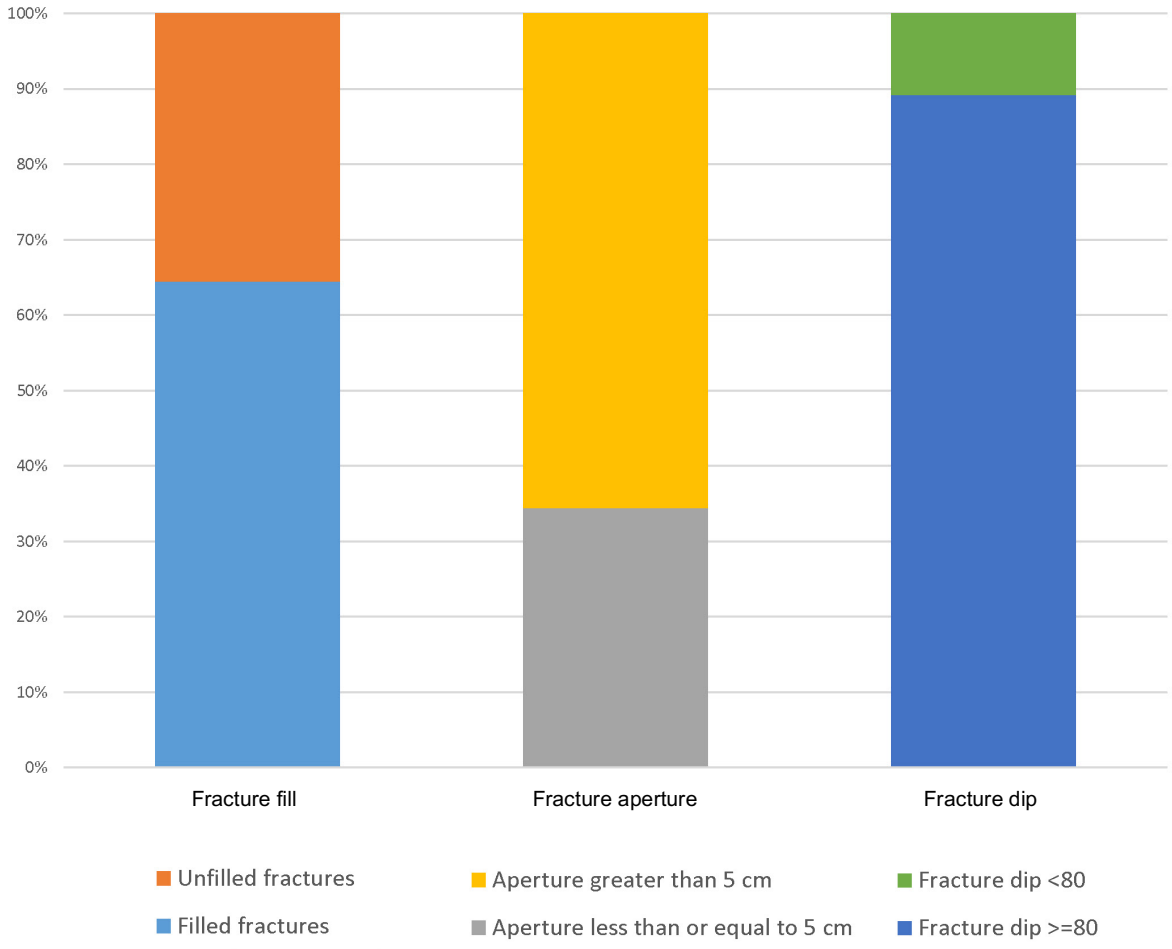

Figure 5-2. 100% stacked column histogram of fill, aperture, and dip angle of sackungen.

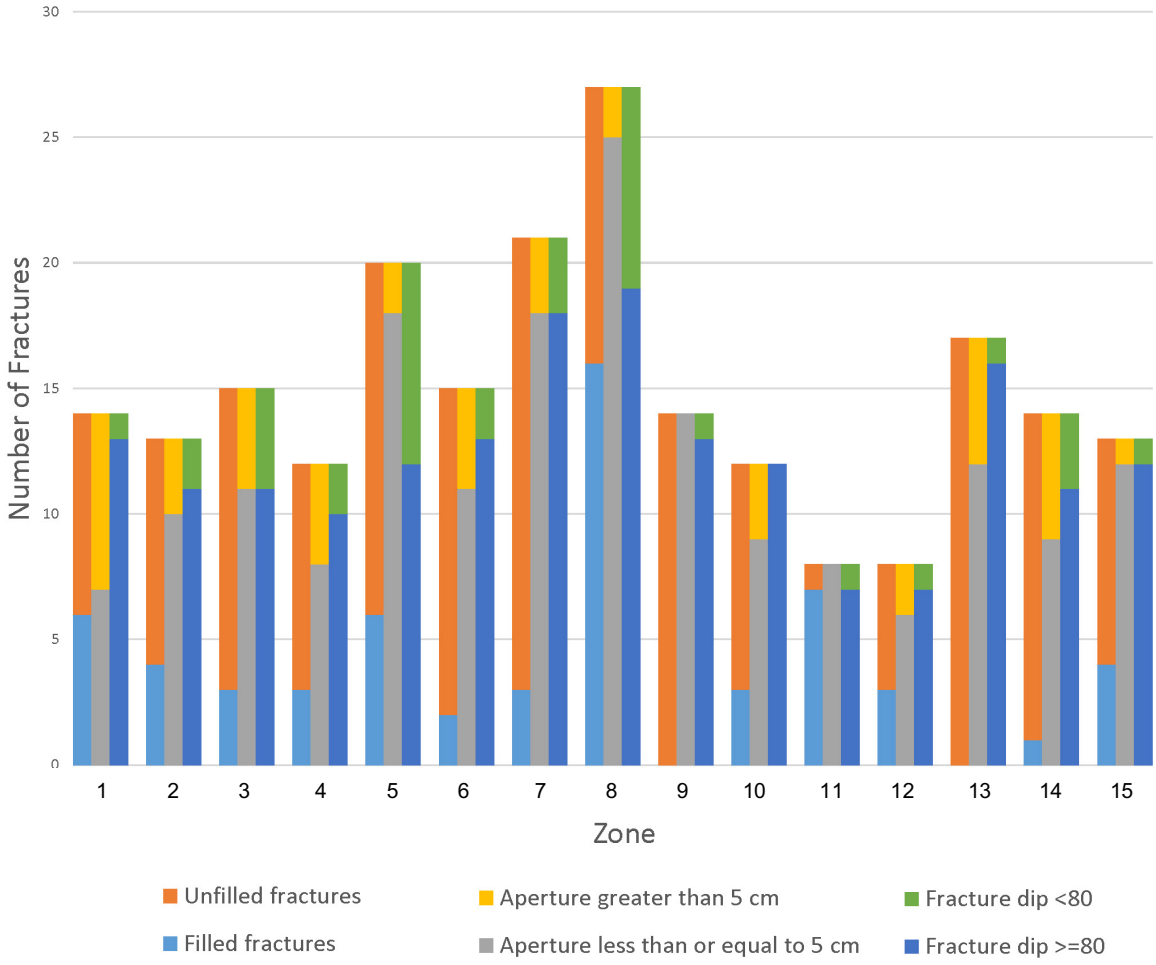

Figure 5-3. Fill, aperture, and dip angle of cliff face fractures for the zones shown in Figure 4-2.

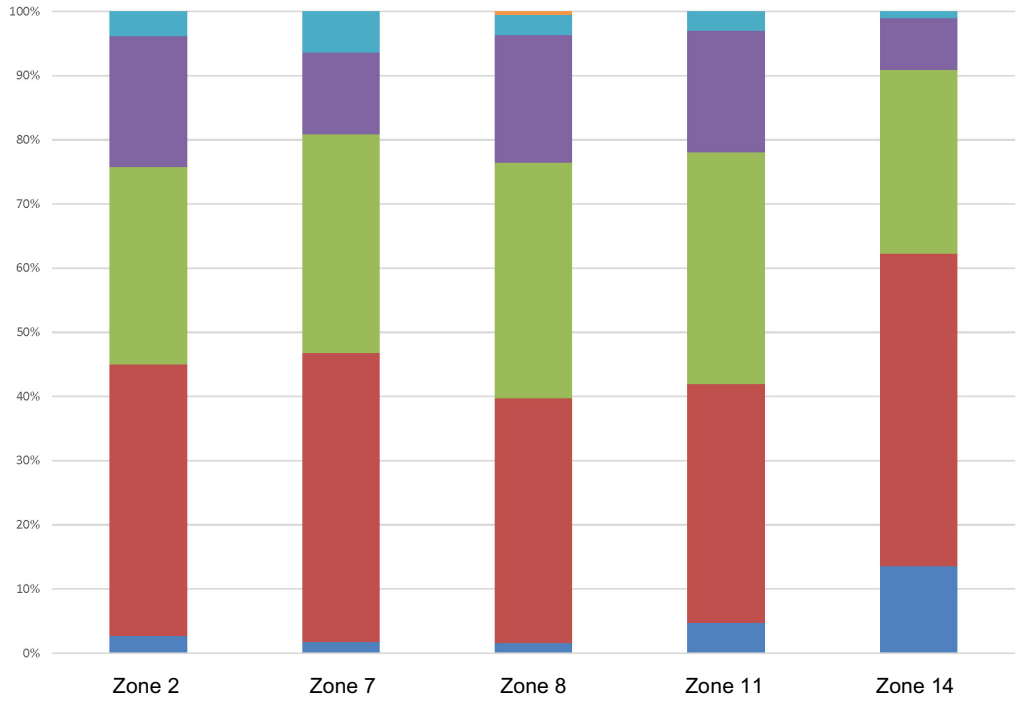

Figure 5-4. 100% stacked column histogram of block fall dimensions. The number of blocks measured in each zone (Figure 4-2) is shown in Table 5-1; the number of blocks in each category is converted into a percentage for this plot. The legend represents measurements in m^3.

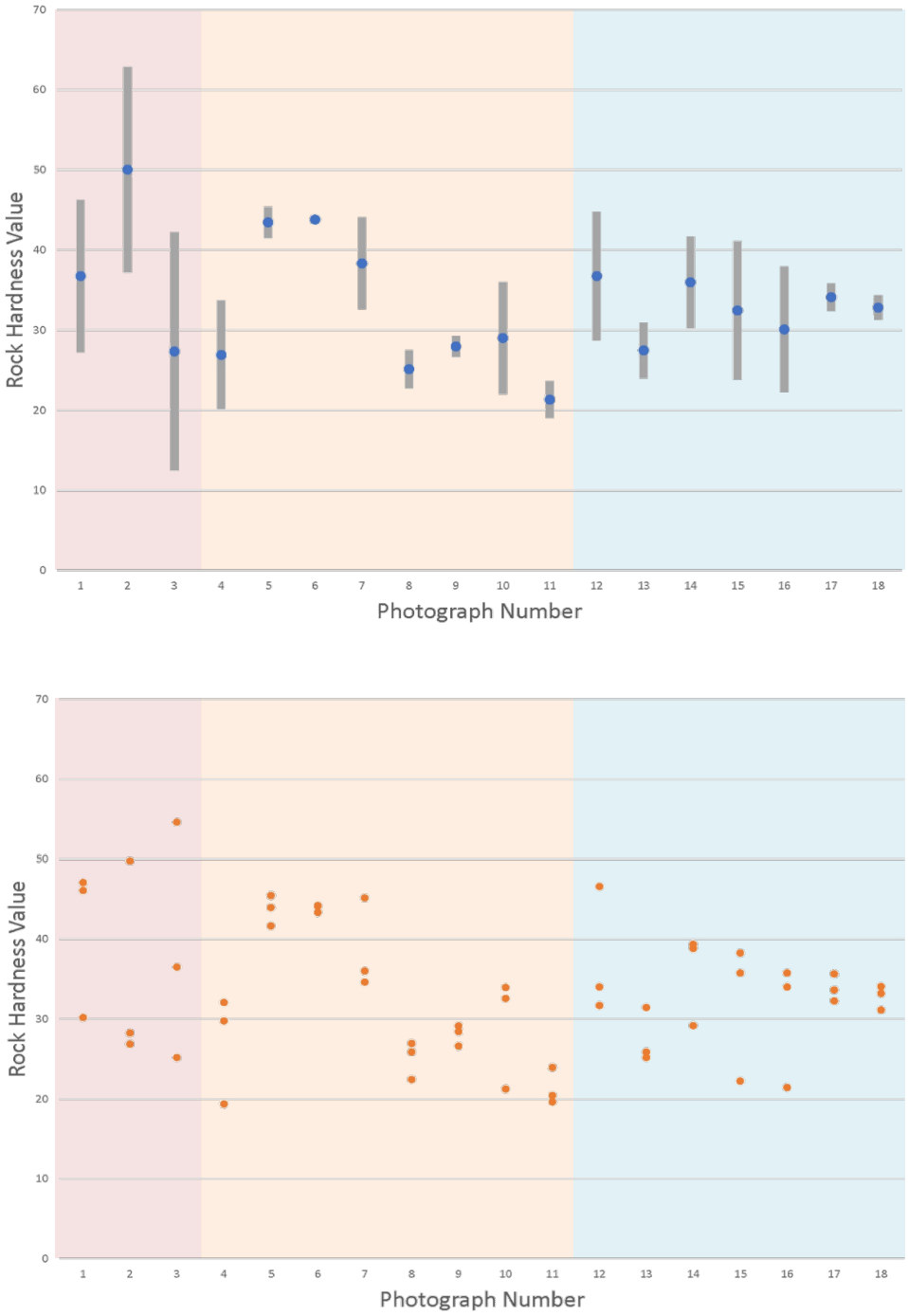

Figure 5-5. (Top) Mean rock hardness calculated using the trimmean *statistical analysis in Microsoft Excel. The x-axis corresponds to the photographs in Figure 5-6. Gray bars represent 1 standard deviation error. The red shading represents rocks classified as "light," beige shading indicates rocks classified as "tan to gray," and blue shading represents rocks with desert varnish. (Bottom) Rock hardness value for each of the three rounds of Schmidt hammer analyses calculated using the* trimmean *statistical analysis.*

Figure 5-6. Photographs of the Schmidt hammer sample locations. Photograph number (in upper left corner of each photograph) corresponds to the number in the x-axis of the plots in Figure 5-5.

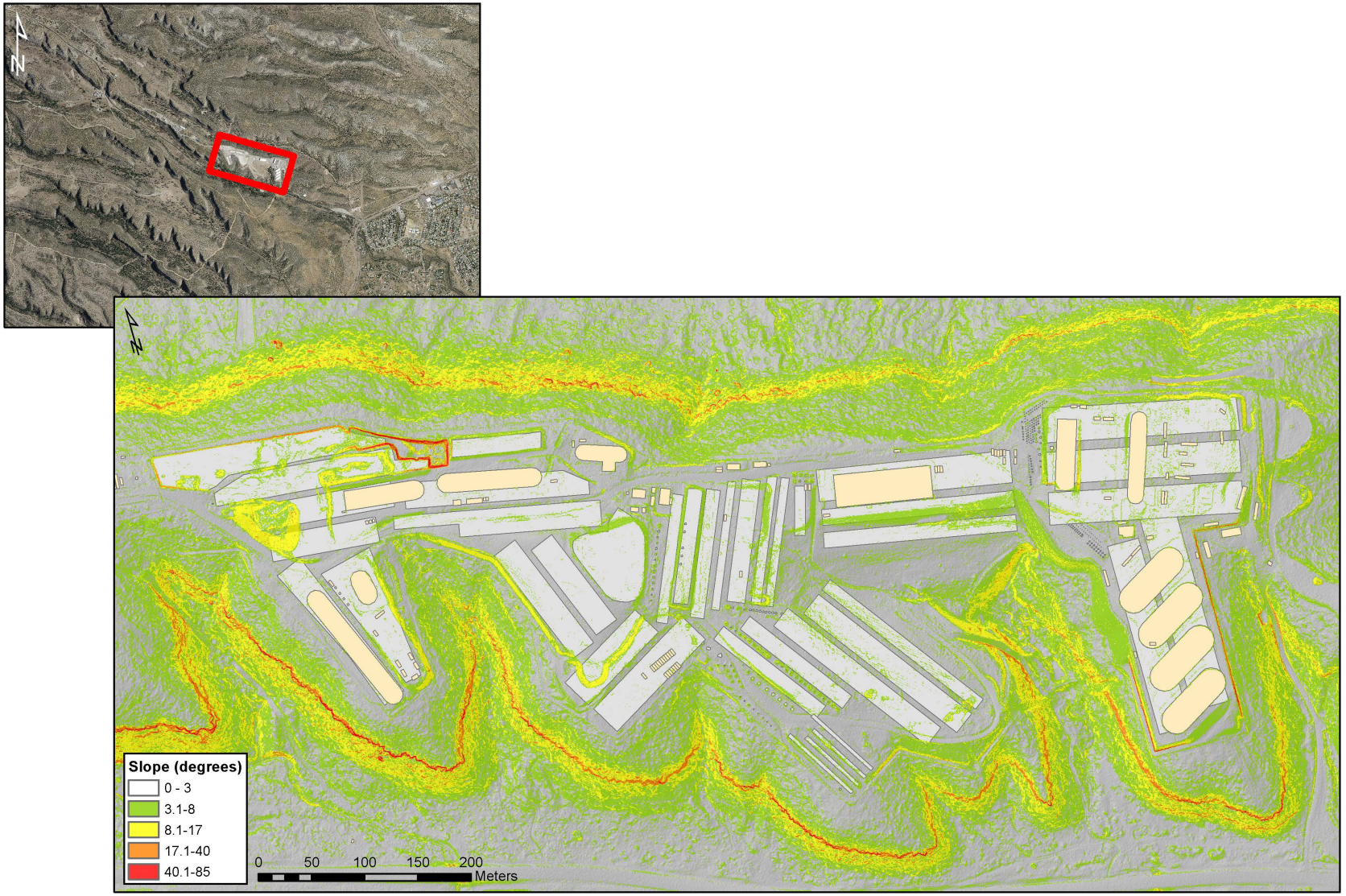

Figure 5-7. Slope angles surrounding MDA G. Green represents shallow-dipping slopes; red indicates steeper slopes (>23°).

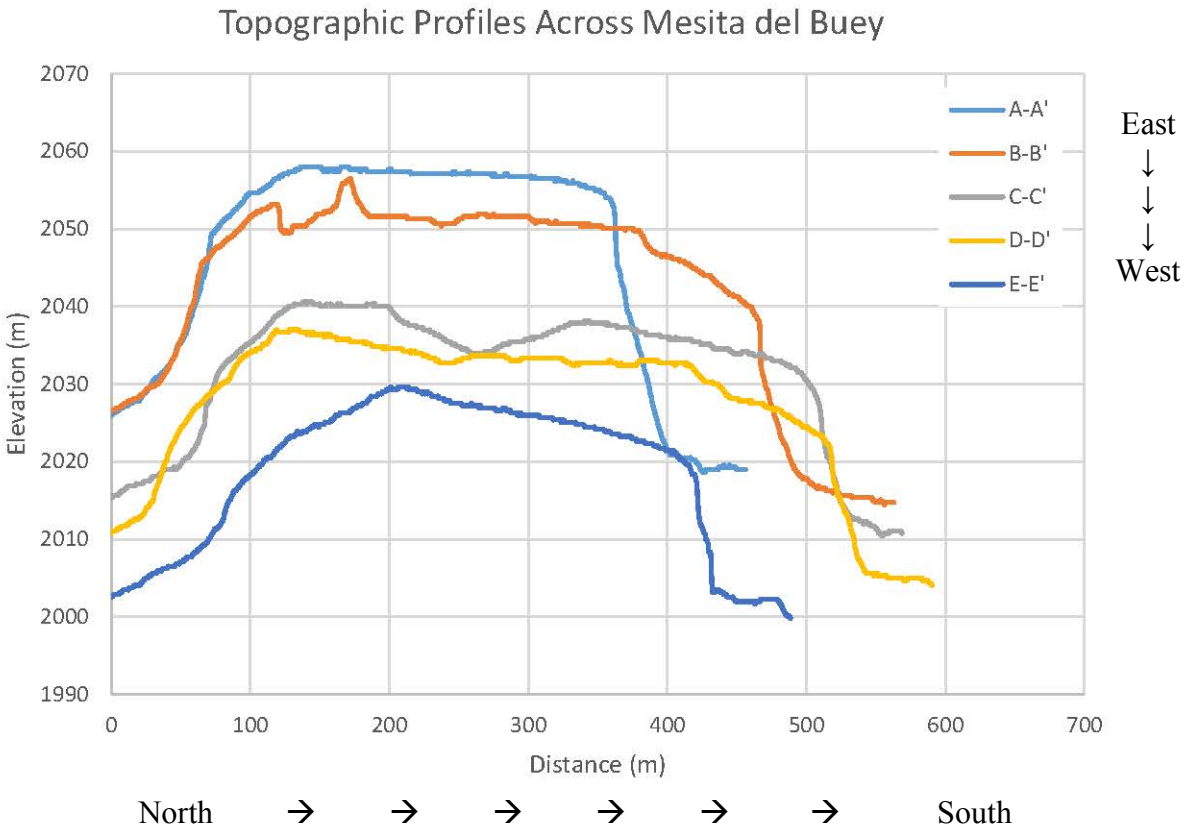

Figure 5-8. Topographic profiles of MDA G from north to south. Refer to Figure 4-7 for cross section line location. The north-facing slopes have shallower slope angles and less relief than the north-facing slopes; additionally, relief and elevation decrease across the mesa (from west to east).

Figure 5-9. Rock art at MDA G. (Left) The fracture is used as a bounding feature for the rock art. (Middle) The fracture (white arrow) intersects the rock art (black arrow) and likely post-dates the rock art. (Right) The bottom of the rock art (red box) has been eroded and washed away.

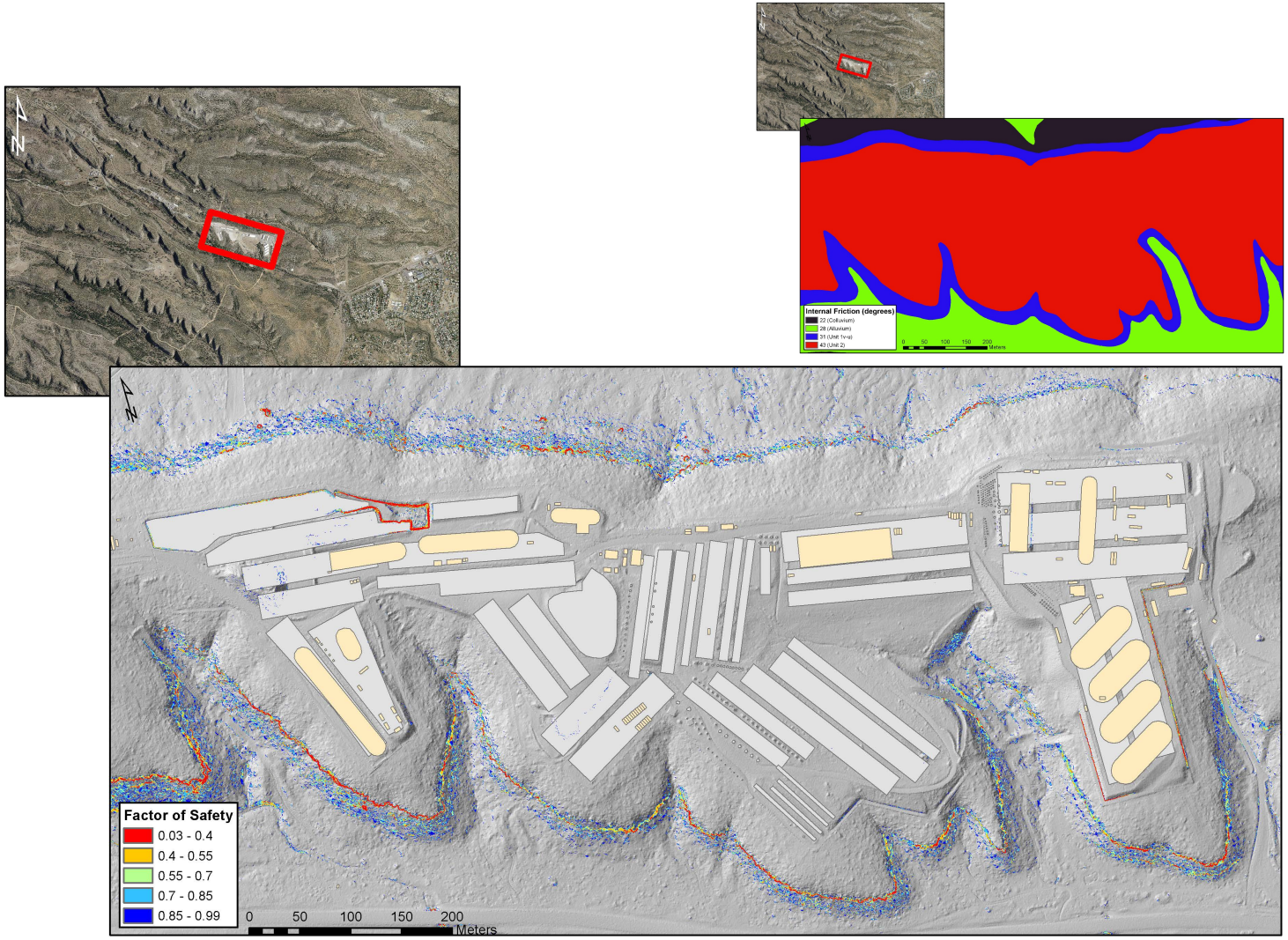

Figure 5-10. (Top) Angle of internal friction map, used during calculation of the FoS. (Bottom) Results of the FoS calculations. Red indicates very low FoS values; blue is higher FoS values (but still less than 1).

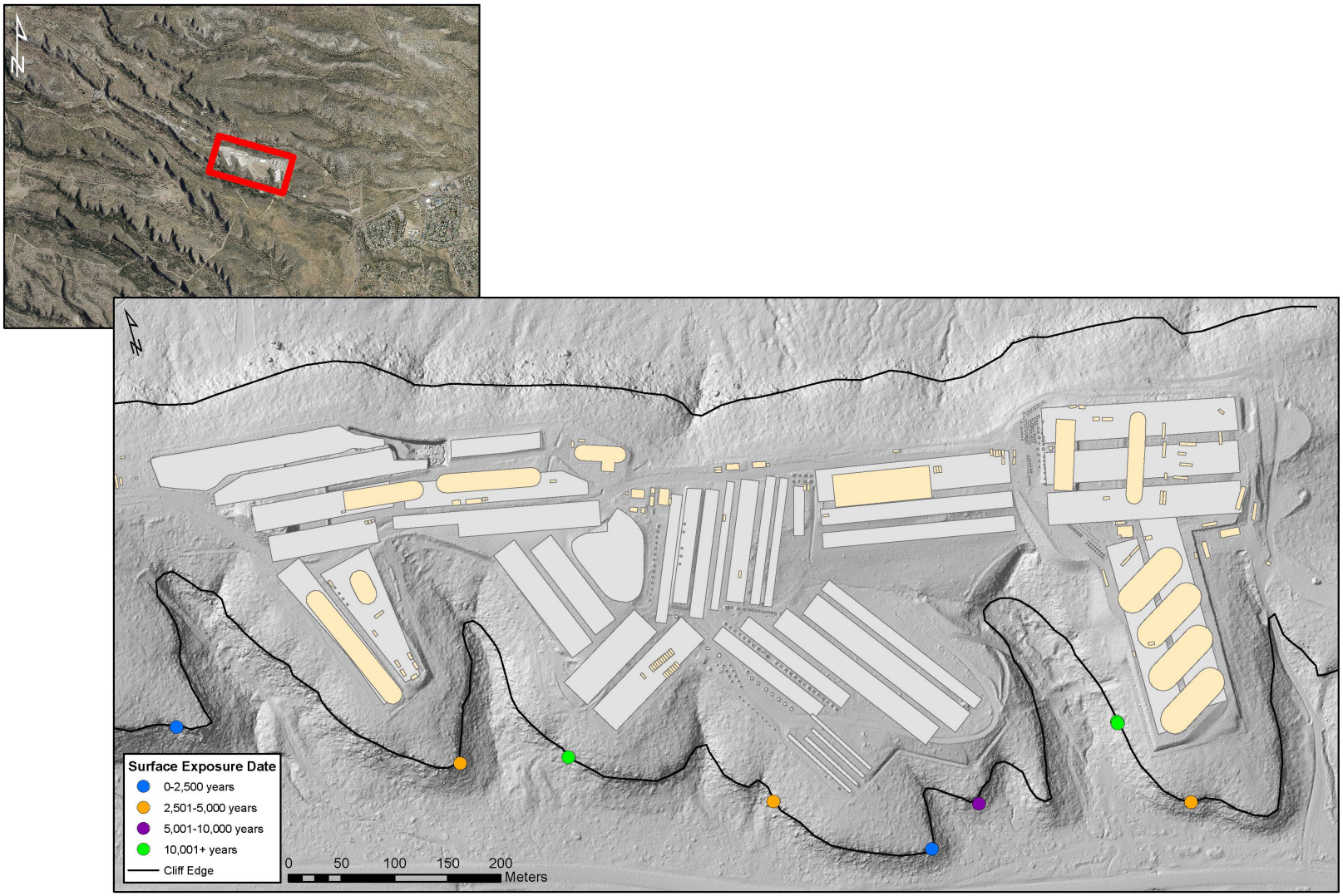

Figure 5-11. Cosmogenic nuclide dating results.

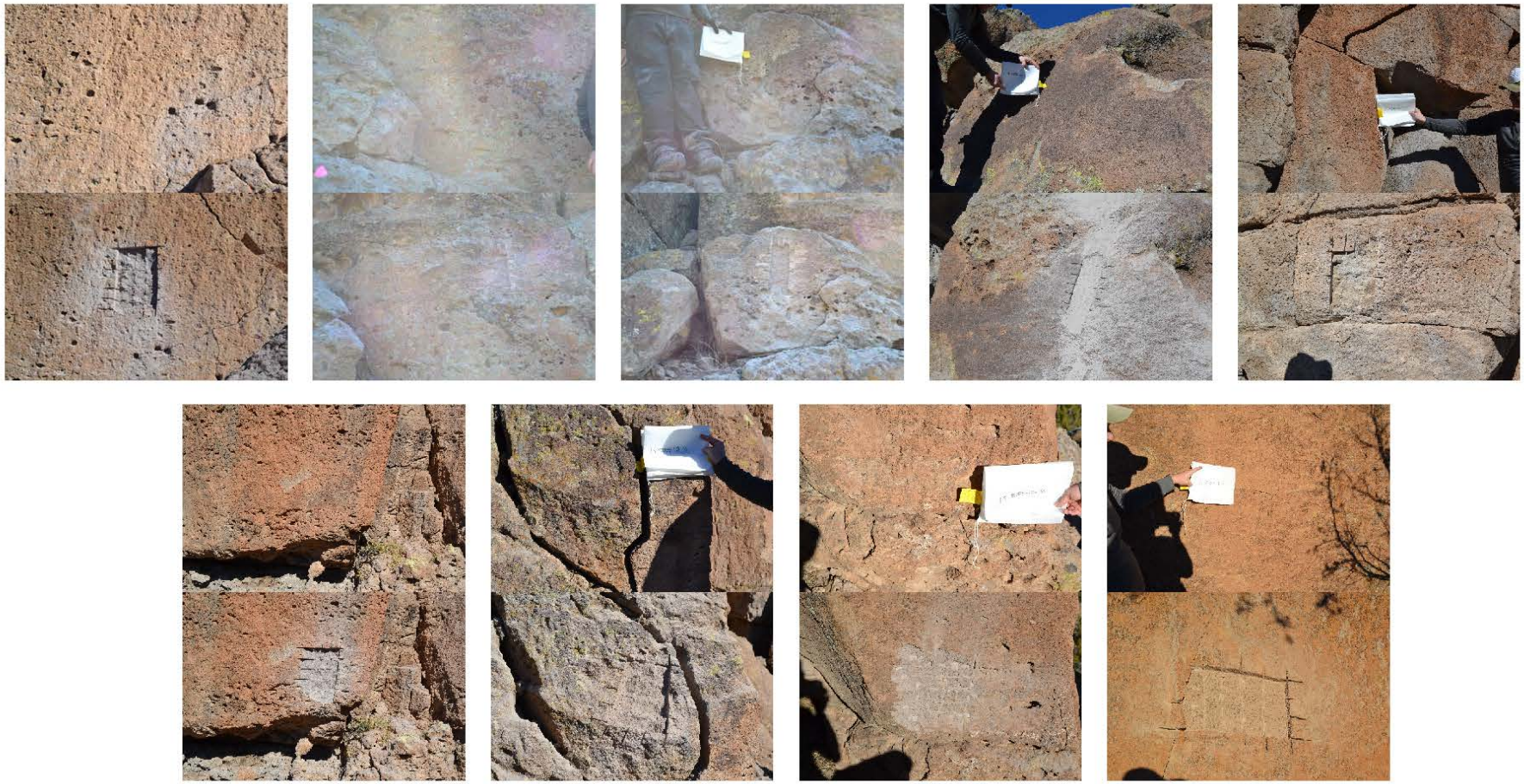

Figure 5-12. Cosmogenic sample locations. Top row, left to right: sample number 1, 2, 3, 4, 5; bottom row, left to right: sample number 8, 10, 12, 14.

6.0 Discussion

The observations and data collected during this investigation, as well as past work, indicate that cliff retreat is actively occurring along Mesita del Buey with the south slope being more susceptible to cliff retreat than the north slope. Quantification of the rate of retreat is essential for assessing the long-term performance of the Area G disposal facility.

6.1 Evidence of Cliff Retreat and Vulnerability to Failure

Existing block falls indicate past cliff failures, while fracture bounded blocks, particularly along the south facing slopes of Mesita del Buey, attest to the potential for continued failure. In particular, the presence of *sackungen* along the mesa-top create a region of weakness between the cliff edge and the fracture. In areas where *sackungen* are offset by 5 meters or more from the cliff edge, a substantial amount of material would fail in a single cliff retreat event.

The results of the fracture mapping and the block fall characterization provide insight into the potential magnitude of future cliff failures. The fracture mapping results indicate that the fractures closest to the cliff edge along the south side of TA-54 lie within 10 m of the mesa edge. Thus, if failure occurs along these fractures, as much as 10 m of material could be lost. Losses of this magnitude, however, are not supported by the results of the block fall characterization. The results from that effort found blocks had a maximum dimension that was generally 2 m or less. The lack of correlation between the large offset of the *sackungen* from the cliff face and the boulder measurements may have two causes. First, the possibility exists that the blocks break apart as they tumble and fall into the canyon. The rocks very close to the cliff edge are highly fractured and may break into smaller pieces, yielding blocks that are much smaller than the rocks whose sizes are inferred from the offset of the *sackungen*. The second possibility is that rather than one large cliff failure event, a large portion (as much as 10 m) of the cliff fails over a relatively short period of time as a result of a series of small failures that are clustered together. The time scale of serial failures could be on the order of days to years.

Table 6-1 provides the details for each zone, including fracture spacing, average fracture aperture, and relative degree of stability (cf. Figure 4-2). Relative stability categorizations were estimated based on analyzing fracture spacing and average fracture aperture. Based on work conducted by Bieniawski (1989), zones with a fracture spacing of 2 m or less were considered to be at a higher risk of failure (lower degree of stability) as were zones whose average fracture apertures were greater than 5 cm. Using these criteria, zones were assigned a rating of low, medium, or high failure risk (Figure 6-1).

Table 6-1. Relative stability of each zone as calculated using fractures and fracture aperture.

Zone	Total no. of fractures	No. of fractures per meter	Average fracture aperture (cm)	Relative risk of failure	Cosmogenic dating sample number, age & rock condition
1	14	2.1	6.4	Moderate	4; 8802 ± 221 yr; competent rock
2	13	2.3	4.3	Low	5; 2391 ± 50 yr; poorly welded, crumbling
3	15	2.0	5.5	High	
4	12	2.5	4.9	Low	8; 3992 ± 81 yr; soft and easy to cut
5	20	1.5	2.8	Moderate	
6	15	2.0	4.1	Moderate	
7	21	1.4	3.9	Moderate	10; 10633 ± 301 yr; varnished and weathered
8	27	1.1	2.9	Moderate	
9	14	2.1	2.6	Low	
10	12	2.5	4.1	Low	12; 4267 ± 87 yr; competent rock, difficult to cut
11	8	3.8	2.9	Low	
12	8	3.8	3.1	Low	
13	17	1.8	3.4	Moderate	1; 3305 ± 68 yr; soft and easy to cut
14	14	2.1	4.9	Low	2 & 3; 12535 ± 408 yr, 12542 ± 407 yr; eroded and toppled boulders
15	13	2.3	3.2	Low	

While these relative values can be useful, they are only moderately correlated with the cosmogenic nuclide dating results. For example, zone 14 has consistent results: two cosmogenic-dating samples with the oldest exposure dates and a low risk of failure (Table 6-1). Conversely, zone 2 has a low risk of failure, but the cosmogenic sample from within zone 2 was noted as being poorly welded and crumbling and had one of the youngest exposure dates. This variation is likely due to the fact that the cosmogenic dating samples are at a much smaller scale than the larger-scale, averaged measurements.

An effort was made to relate the hardness of the rocks comprising the cliff faces to the color of the faces. In this approach, color was used as an indication of the age of the cliff face, or the period of time the face has been exposed to the environment and weathering. Others (e.g., McCarroll, 1991; Betts and Latta, 2000) have demonstrated correlations between hardness of rocks and the degree

of weathering they have undergone. The development of similar correlations for the cliffs along TA-54 could prove useful in terms of estimating rates of cliff retreat. However, there were no apparent correlations between the colors of the rock faces at Area G and the hardness measurements conducted using the Schmidt hammer. Whereas light-colored (less weathered) faces yielded higher rebound coefficients in some cases, the opposite was also true. The presence of lichens may have complicated the interpretation of the data in some cases. Lichens were observed on some of the dark rock faces and may affect rock weathering rates, accelerating weathering under some conditions (Adamo and Violante, 2000) and possibly slowing breakdown of the rock in other cases (e.g., Seaward et al., 1989; Ariño et al., 1995).

Additionally, the results of the cosmogenic surface dating were compared to the sample locations (cf. Figure 5-13) in order to determine a possible correlation between cliff face color and age. Samples 5 and 8 are similar in color, but sample 8 is nearly twice as old as sample 5. Sample 4 and 10 are also similar in color, but sample 4 is nearly 2,000 yr younger than sample 10. Non-co-located samples that are closest in age (samples 8 and 12) are also not similar in color.

The 22-month photodocumentation campaign detected no areas of change. Generally, this technique was not very useful in long-term cliff retreat quantification, since visual inspection of photographs will only detect changes on the cobble to boulder (or larger) scale. However, since the start of this study, high-resolution surface characterization techniques such as Lidar surveys have become cheaper and more commercially available. In 2014, LANL contracted with Atlantic Group to collect airborne Lidar over the entire LANL footprint. Lidar is a remote-sensing technique that uses a pulsed laser to measure distance to the surface. The result of this Lidar collection is a DEM with 0.3 m resolution. Additionally, through the use of photogrammetry software (e.g., AgiSoft), legacy photos of TA-54 from the early 1960s were used to produce a historical DEM of MDA G. The resultant DEM is 0.4 m resolution.

To better assess decadal change at MDA G, the ArcGIS plug-in Geomorphic Change Detection (Wheaton et al., 2010) was used to create a DEM of Difference (DoD)(Figure 6-2). The first step was to match the resolutions of both the historical and the 2014 DEM; this was done by using the ArcGIS tool *Resample* to produce a 2014 DEM with 0.4 m resolution. Then the historical imagery was subtracted from the 2014 LANL Lidar DEM to produce a DoD. The substantial modification that has taken place on Mesita del Buey is obvious, where waste disposal and capping activities have generally increased the surface elevation. However, changes in the cliffs are less obvious. While some change is detected, particularly in the south-facing cliffs, a rigorous error analysis would need to be performed in order to take into account the inherent errors associated with the surface elevation collection methods (Wheaton et al., 2010).

The north and south slopes of Mesita del Buey are distinctly different in terms of topography and vegetation. Configurations of the two slopes are a reflection of the past impacts of erosion and cliff

retreat and will likely influence the mesa's vulnerability to cliff retreat in the future. The shadier conditions on the north slow water evaporation, allowing the soils to retain snow and moisture from rainfall for longer periods. In contrast, south-facing slopes receive more direct sunlight and experience more rapid evaporation, leading to less favorable growing conditions for plants. Fractures provide isolated locations for water to collect, allowing limited footholds for vegetation.

In addition, the accumulation of snow on the north-facing slopes leads to higher and more prolonged rock moisture levels, which support higher rates of chemical weathering (Hall, 1993). These processes have contributed to a general breakdown of the cliffs, stabilizing the north side by reducing topographic relief and creating gentler colluvial slopes; the vegetation that becomes established because of the more favorable growing conditions contributes to this stability. The overall slope of the cliffs is close to its angle of repose, making the northern side of Mesita del Buey less prone to cliff retreat in the future.

6.2 Rates of Cliff Retreat

Cliff retreat along the north and south slopes of Mesita del Buey will lead to the narrowing of the mesa over time. Rates of retreat specific to Area G had not been developed before this investigation, but the rate will ultimately determine the threat posed by block fall to the long-term performance of the Area G disposal facility. As calculated in Section 5.4, Mesita del Buey will narrow by approximately 2.4 to 4.4 m every 10,000 years. Using these cliff retreat rates and assuming a 15-m setback for the disposal units at Area G, the time required to disrupt the disposal units ranges from 34,000 yr to 62,000 yr .

However, Earth and earth processes are not average, but rather punctuated and episodic. Surface exposure dating provides essential dating results that provide insight into more recent failure events. Table 6-2 is a compilation of the cosmogenic nuclide dating studies that have been completed at TA-54. Cosmogenic nuclide dating consistently reports slower erosion values than the erosion estimate based on average canyon widening rates.

Table 6-2. Comparison of erosion rates per 10,000 years for various dating techniques.

Reference	Method	Erosion Rate per 10,000 years
Purtymun and Kennedy (1971)	Not specified	140 cm
Poths and Goff (1990)	He and Ne cosmogenic dating	18 cm (densely welded units) 28 cm (less densely welded units)
Albrecht et al. (1993)	Be and Al cosmogenic dating	1 cm (densely welded units) 11 cm (less densely welded units)

This study	C-14 cosmogenic dating	145.5 cm (densely welded units, median value) Range of 27.6 to 347.7 cm (densely welded units)
This study	Average canyon widening measurements	260 to 440 cm

Combining mean block size, fracture spacing, and exposure dates at each sample location can provide an estimate of how long it will take for a specific cliff location to retreat enough to expose a disposal pit or shaft. At each site, blocks and fractures at the edge of the cliff are digitized using ArcGIS. Measuring the distance to the closest disposal site and assuming that failure will continue to occur at the same rate as the cosmogenic dating age, it is possible to estimate how long it will take for retreat to lead to pit or shaft exposure (Figure 6-3). This calculation was done at three different locations and yielded estimates ranging from 108,000 to 328,000 yrs.

Figure 6-4 assesses the possible relationship between surface dating results and slope characteristics such as flow direction and aspect. If a relationship can be established between certain slope characteristics and the most recent failure event, this would help identify areas at greater risk for failure. However, at this point, no relationship seems to exist.

6.3 Seismic Activity and Quantification of Cliff Retreat during Seismic Events

Seismic activity, if severe enough, may cause the formation of fractures in the cliffs lining TA-54 or facilitate the failure of blocks that have already undergone fracturing. The 50 km long Pajarito fault system that extends along the western margin of the Laboratory is the dominant contributor to seismic hazard at the Laboratory because of its proximity and level of activity (Wong et al., 1995; Wong et al., 2007). The fault system exhibits rupture patterns and shows evidence of at least two, probably three, surface-faulting earthquakes in the past 11,000 yr (Gardner et al., 2003; Lewis et al., 2009; Schultz-Fellenz et al., in prep.; Wong et al., 1995; Wong et al., 2007).

A site-specific seismic hazard analysis does not exist for TA-54. However, data collected during this investigation may be used with other sources of information to approximate the ground motion required to trigger cliff retreat and, in turn, the minimum earthquake magnitude necessary to generate the required ground motion. The estimates presented below are approximate at best and should be confirmed by a more thorough ground motion analysis for the site.

Although the unit 2 cliffs are inherently unstable and do not require external forces to fail, the minimum earthquake magnitude required to cause block fall provides insight into the risk posed by seismic activity to the cliffs along TA-54. Estimating the ground motion necessary to trigger block failure requires the use of the FoS to calculate the critical acceleration for failure. The critical peak ground acceleration necessary to initiate block fall is given by (Newmark, 1965):

$$A_c = (FS-1)\sin(\alpha) \quad (3)$$

Where

A_c = critical acceleration for failure (units of *g*, acceleration due to Earth's gravity)
α = slope of the cliff or block face

This calculation treats a cliff as a rigid-plastic body, with no internal deformation, and assumes failure occurs along a discrete shear surface when the critical acceleration is exceeded (Jibson, 1993). This is consistent with cliff failure at TA-54, in which a block fails along a discrete fracture surface as one large mass, with no internal deformation.

The resulting value of A_c is used to calculate the Arias intensity, a ground motion parameter that expresses the potential destructiveness of an earthquake as the integral of the square of the acceleration-time history (Arias, 1970). The Arias intensity is determined as follows (Jibson and Keefer, 1993):

$$I_a = 0.9\ T\ A_c^2 \quad (4)$$

Where

I_a = Arias intensity (m/s)
T = Dobry duration (s) (Dobry et al., 1978), the time required before the Arias Intensity reaches 90% of the maximum

For this study, a Dobry duration of 10 s was used; this is similar to the Dobry durations calculated for California earthquakes of similar hypocenter and magnitude as quakes on the Pajarito Fault System.

Wilson and Keefer (1985) developed a simple relationship between Arias intensity, earthquake magnitude, and source distance:

$$\log I_a = M - 2\log R - 4.1 \quad (5)$$

Where

R = distance from epicenter of earthquake (km)

This equation can be used to estimate the earthquake magnitude that could produce enough ground acceleration to trigger block failure at TA-54. The peak ground acceleration hazard to all sites at the Laboratory is dominated by the Pajarito fault system (Wong et al., 2007); the distance from that fault to the eastern end of MDA G is approximately 11 km (6.8 mi). The results of these calculations are shown in Figure 6-5.

A comparison of the cosmogenic dating samples and the approximate date ranges for surface-faulting earthquakes in the last 11,000 yr (Figure 6-6) does not indicate a direct link between seismic and cliff failure events. However, some studies (e.g., Duan and Oglesby, 2005) have suggested that during faulting events, the horizontal component of ground motion dominates on the footwall, while the vertical component dominates on the hanging wall. MDA G is located on the hanging wall of the Pajarito Fault System, and therefore might experience less horizontal acceleration. This could explain the lack of correlation between seismic events and cosmogenic dates, although more cosmogenic samples could refine this analysis. Additionally, the Laboratory is currently undergoing an update to its seismic hazard analysis, which could refine the date ranges of the most recent events.

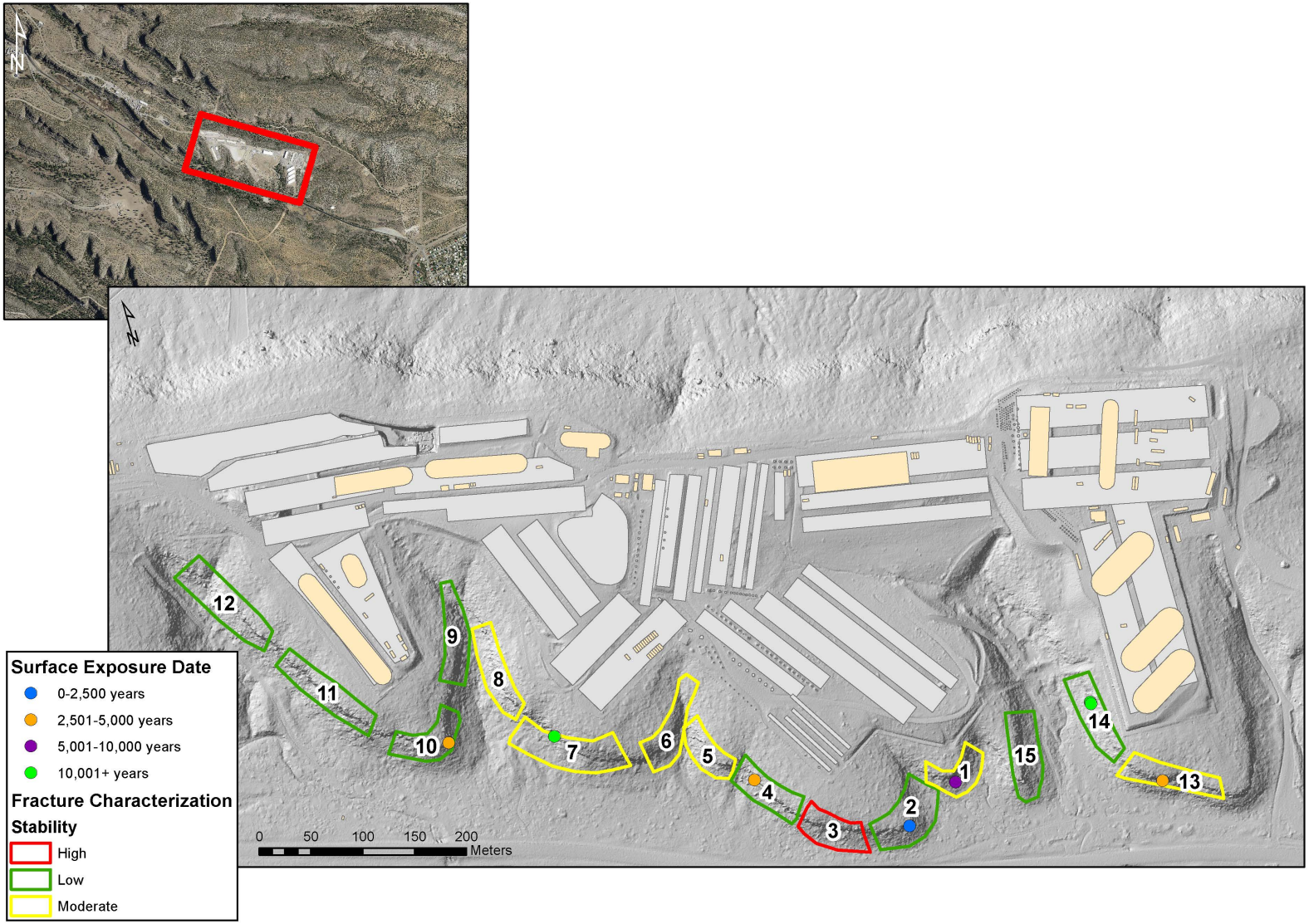

Figure 6-1. Comparison of failure risk calculated using fracture spacing and aperture to cosmogenic nuclide dating results.

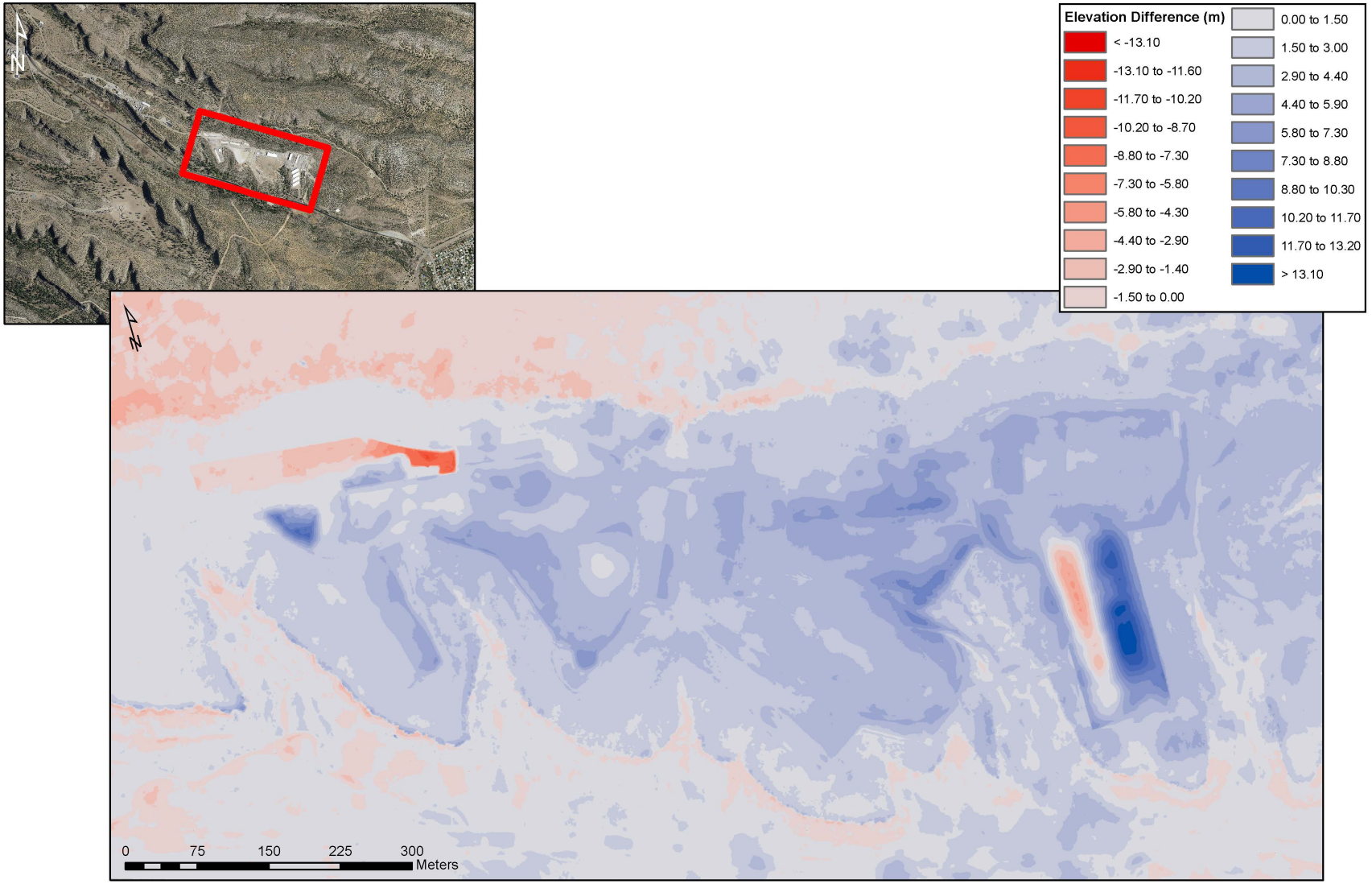

Figure 6-2. Change detection results for MDA G. The DEM produced from the historical imagery was subtracted from the new DEM produced from the 2014 LANL Lidar. Red represents erosion or surface excavation, and blue represents deposition or surface/infrastructure modification.

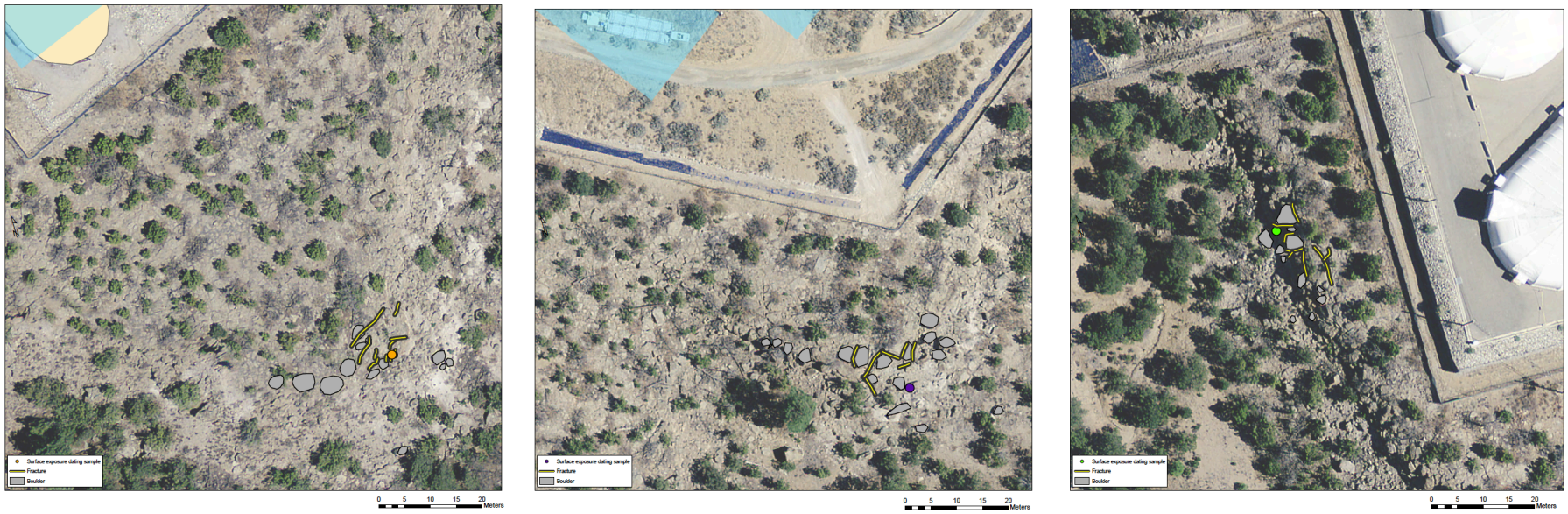

Figure 6-3. Blocks (gray) and fractures (yellow) have been digitized in ArcGIS using the aerial imagery. Assuming that failure continues to occur at the same rate as the surface exposure dating in that location, an estimate can be derived for how long it will take for retreat to lead to exposure. (Left, west) 108,000 years. (Middle, central) 328,000 years. (Right, east) 233,000 years.

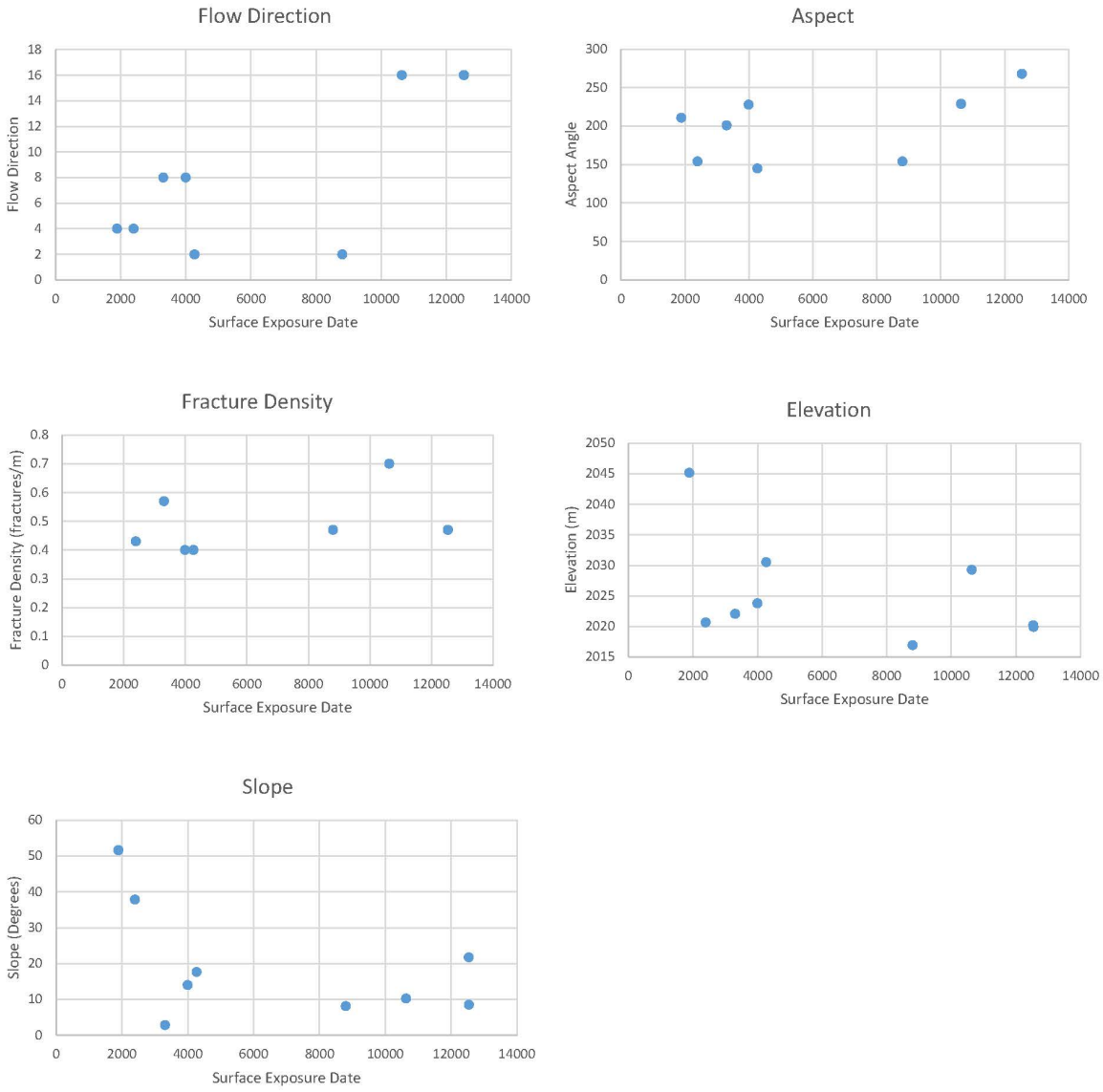

Figure 6-4. Slope characteristics as calculated in ArcGIS (flow direction, aspect, elevation, and slope) or field work (fracture density) compared to cosmogenic exposure dates.

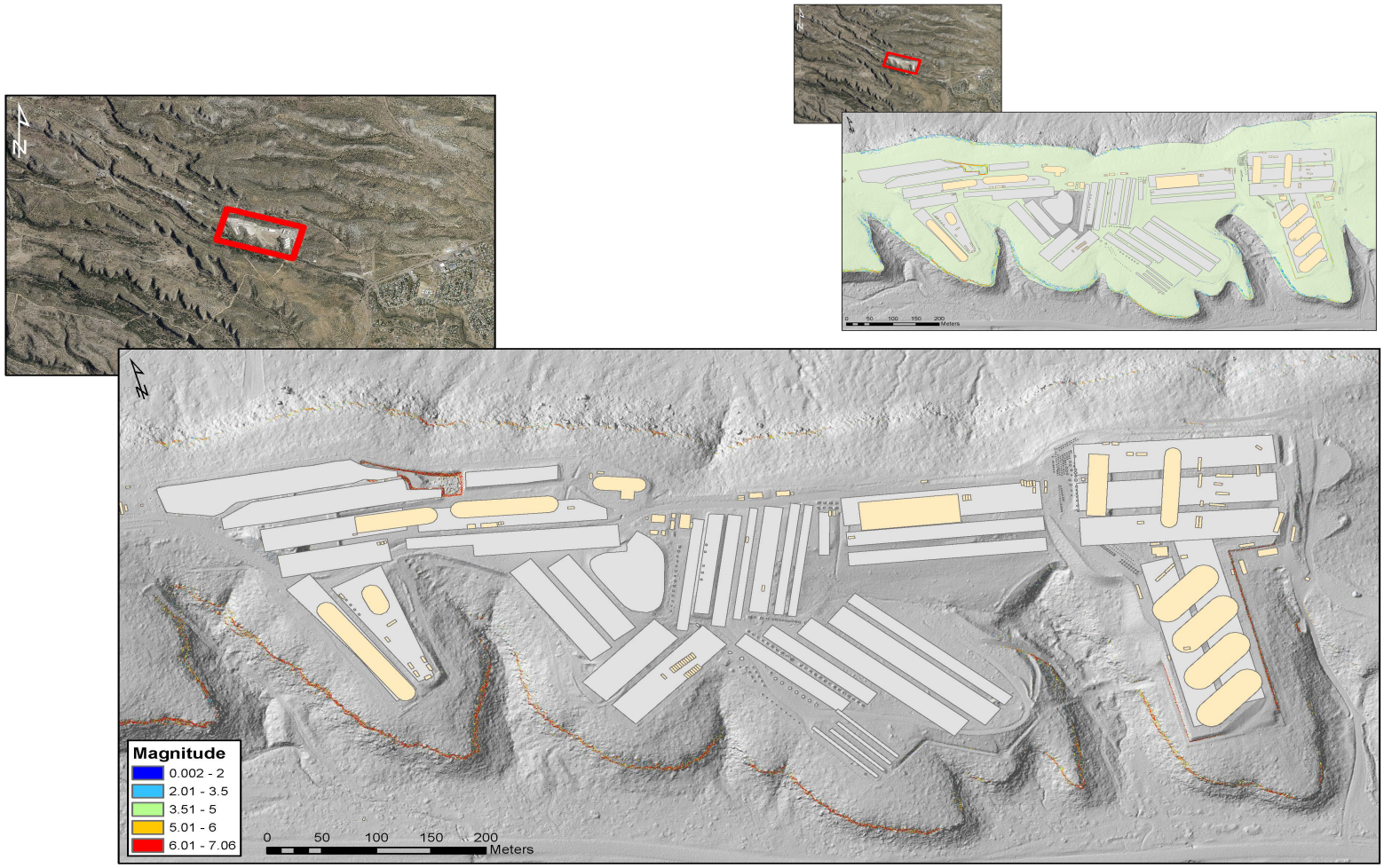

Figure 6-5. Earthquake magnitude required to generate enough ground motion for cliff failure to occur. (Top) The FoS results have been clipped so that the only values being used for the earthquake magnitude calculation are in unit 2 (shown in green). (Bottom) Results of the magnitude calculations.

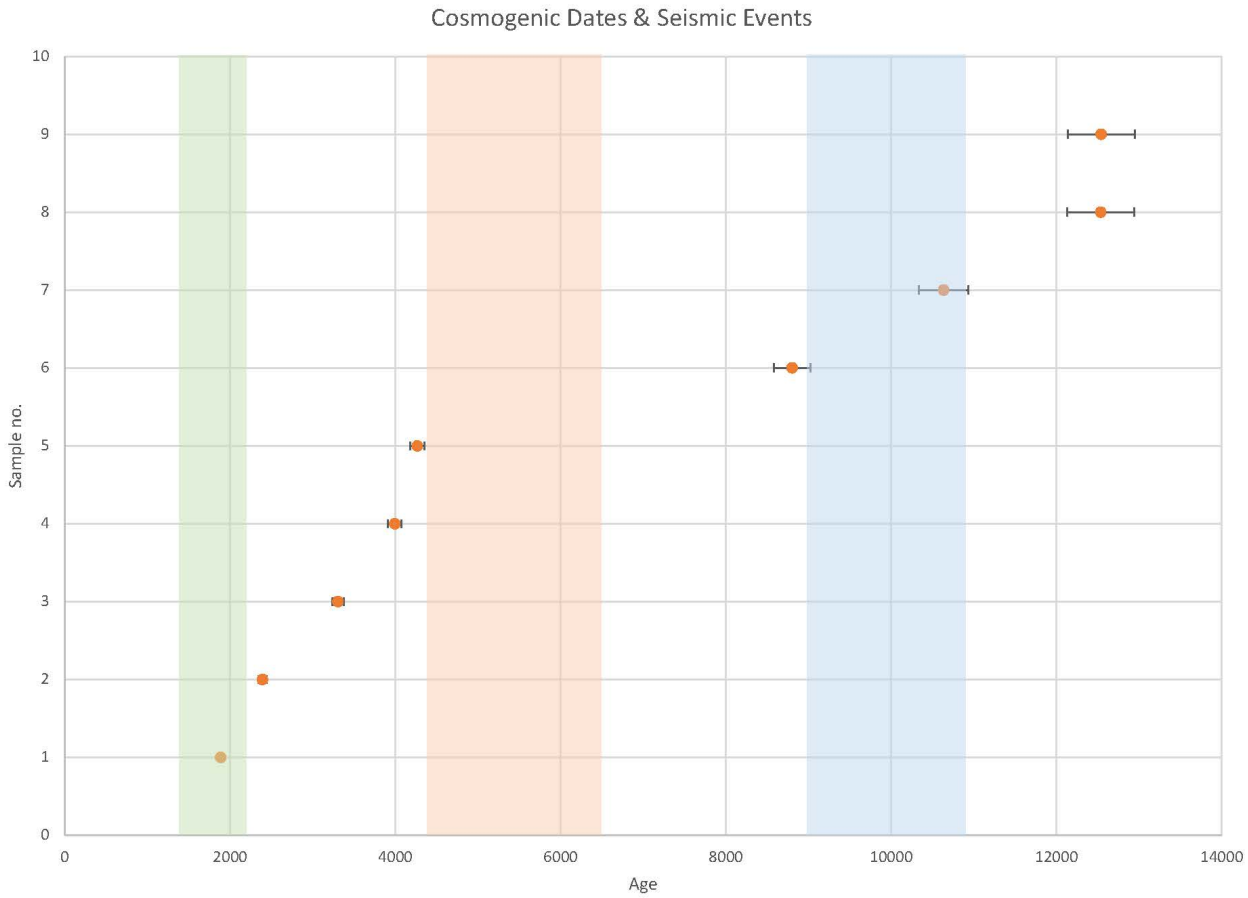

Figure 6-6. Relationship between cosmogenic exposure dating results and large seismic events on the Pajarito Fault System.

7.0 Conclusions

Cliff retreat is actively occurring at TA-54, and continued cliff failure will ultimately expose pits and shafts at MDA G. In particular, large mesa-top fractures spaced at intervals of 1 m or greater create a zone of failure along which large block falls have occurred and are expected to propagate into the future.

Surface exposure dating results show that block failure has occurred within the last 10,000 yrs, but typical block failure events will only result in cliff retreat of 2 to 5 m in a single block fall event. Combining these surface exposure dates with average block fall sizes results in potential pit or shaft exposure anywhere between 108,000 to 300,000+ yrs in the future. These erosion rates and subsequent exposure calculated using surface exposure dating yield results very similar to those of Purtymun and Kennedy (1971).

Many of the youngest surface exposure dates are locations where the cliff face creates a prominent southeast-facing "nose", while the oldest surface exposure dates are located in side drainages where extensive erosion and surface modification has occurred in the past. The distribution of these ages suggests slower future erosion in the side drainages and faster erosion on the prominent noses, but more samples are needed to fully assess this hypothesis.

FoS calculations to determine the magnitude required to cause cliff failure calculated a magnitude of 5 or higher to trigger a retreat event. However, surface exposure dates did not show a strong correlation with past seismic events. An update to LANL's Probabilistic Seismic Hazard Analysis (PSHA) is currently underway and could provide refined ages that are more closely linked to cliff failure.

7.1 Future Work

Continued research and data collection at MDA G can provide additional insight and data points to use for refining the initial estimates of cliff retreat rates calculated in this report.

Surface exposure dating: Surface exposure dating on the north side and additional dating on the south side will supplement existing surface exposure dating results to identify the areas at greatest risk of future failure and retreat events. With the addition of more surface exposure dates, these data can be incorporated into models of the proposed MDA G cover and future erosion in order to determine locations that should be reinforced.

Repeat Lidar surveys: Current drone-based photogrammetric surveys being deployed for other LANL projects have produced DEMs with sub-centimeter resolution (Schultz-Fellenz et al., 2017). Conducting Lidar surveys at regular intervals (seasonal to start, then yearly) can improve change detection analyses and identify fracture widening and areas of concern over time.

Crack meters: The installation of crack meters, along with temperature, light, and humidity sensors (Collins and Stock, 2016), will provide essential diurnal and seasonal measurements of fracture widening. These data can also be incorporated into erosion models to identify locations at greater risk of failure.

Ground motion during seismic events: The update of LANL's PSHA might provide essential information regarding ground motion on the footwall versus headwall during an earthquake. Incorporating these data, along with additional surface exposure ages, could further refine the effect of ground motion on cliff retreat at MDA G.

8.0 References

Abeele, W.V., Wheeler, M.L., and Burton, B.W., 1981, "Geohydrology of Bandelier Tuff," Los Alamos National Laboratory Report LA-8962-MS, Los Alamos, New Mexico.

Adamo, P., and Violante, P., 2000, "Weathering of rocks and Neogenesis of Minerals Associated with Lichen Activity," *Applied Clay Science*, Vol. 16, pp. 229–256.

Albrecht, A., Herzog, G.F., Klein, J., Dezfouly-Arjomandy B., and Goff, F., 1993, "Quaternary Erosion and Cosmic-Ray-Exposure History Derived from ^{10}Be and ^{26}Al Produced In Situ – An Example from Pajarito Plateau, Valles Caldera Region," *Geology*, Vol. 21, pp. 551–554.

Arias, A., 1970, *A Measure of Earthquake Intensity, Seismic Design for Nuclear Power Plants*, MIT Press, pp. 438–483.

Ariño, X., Ortega-Calvo, J.J., Gomez-Bolea, A., Saiz-Jimenez, C., 1995, "Lichen Colonization of the Roman Pavement at Baelo Claudia (Cadiz, Spain): Biodeterioration vs. Bioprotection," *The Science of the Total Environment*, Vol. 167, pp. 353–363.

Beck, A.C., 1968, "Gravity Faulting as a Mechanism of Topographic Adjustment," *New Zealand Journal of Geology and Geophysics*, Vol. 11, pp. 191–199.

Betts, M.W., and Latta, M.A., 2000, "Rock Surface Hardness as an Indication of Exposure Age: An Archaeological Application of the Schmidt Hammer," *Archaeometry*, Vol. 42, No. 1, pp. 209–223.

Bieniawski, Z.T., 1989, *Engineering Rock Mass Classifications: A Complete Manual for Engineers and Geologists in Mining, Civil, and Petroleum Engineering*, Wiley-Interscience, New York, 251 pp.

Bovis, M.J., 1982, "Uphill-facing (Antislope) Scarps in the Coast Mountains, Southwest British Columbia," *Geological Society of America Bulletin*, Vol. 93, pp. 804–812.

Bowen, B.M., 1990, "Los Alamos Climatology," Los Alamos National Laboratory Report LA-11735-MS, Los Alamos, New Mexico.

Broxton D.E., and Reneau, S.L., 1995, "Stratigraphic Nomenclature of the Bandelier Tuff for the Environmental Restoration Project at Los Alamos National Laboratory," Los Alamos National Laboratory Report LA-13010-MS, Los Alamos, New Mexico.

Broxton, D.E., and Reneau, S.L., 1996, "Buried Early Pleistocene Landscapes Beneath the Pajarito Plateau, Northern New Mexico," *New Mexico Geological Society Guidebook*, 47th Field Conference, Jemez Mountains Region, pp. 325–334.

Broxton, D.E., and Rogers, M.A., 2007, "Comparison of two systems of nomenclature for the Tshirege Member, Bandelier Tuff, central Pajarito Plateau, New Mexico," *Kues, B.S., Kelley, S.A.,*

and Lueth, V.W. (Eds.) Geology of the Jemez Region II, New Mexico Geological Society, 58th Annual Field Conference, Socorro, NM, p. 37-39.

Collins, B.D., and Stock, G.M., 2016, "Rockfall triggering by cyclic thermal stressing of exfoliation fractures," *Nature Geoscience*, Vol. 9, pp. 395-401.

Dethier, D.P., 1996, *Geology of White Rock quadrangle, Los Alamos and Santa Fe Counties, New Mexico*, New Mexico Bureau of Geology and Mineral Resources, Geologic Map 73, Scale 1:24,000.

Dobry, R., Idriss, I.M, and Ng, E., 1978, "Duration Characteristics of Horizontal Components of Strong-Motion Earthquake Records," *Seismological Society of America Bulletin*, Vol. 68, pp. 1487–1520.

Duan, B., and Oglesby, D.D., 2005, "The Dynamics of Thrust and Normal Faults over Multiple Earthquake Cycles: Effects of Dipping Fault Geometry," *Bulletin of the Seismological Society of America*, vol. 95, No. 5, pp. 1623-1636.

Gardner, J.N., and Goff, F., 1984, "Potassium-Argon Dates from the Jemez Volcanic Field: Implications for Tectonic Activity in the North-Central Rio Grande Rift," *in* Baldridge, W., Dickerson, P., Riecker, R., and Zidek, J., eds., *Rio Grande Rift: Northern New Mexico*, New Mexico Geological Society Guidebook, 35th Field Conference, October 11–13, pp. 75–81.

Gardner, J.N., and House, L., 1994, "Surprisingly High Intensities from Two Small Earthquakes, Northern Rio Grande Rift," New Mexico, EOS: Transactions of the American Geophysical Union, Vol. 75, p. 240.

Gardner, J.N., Lavine, A., WoldeGabriel, G., Krier, D., Vaniman, D., Caporuscio, F., Lewis, C., Reneau, P., Kluk, E., and Snow, M.J., 1999, "Structural Geology of the Northwestern Portion of Los Alamos National Laboratory, Rio Grande Rift, New Mexico: Implications for seismic surface rupture potential from TA-3 to TA-55," Los Alamos National Laboratory Report LA-13589-MS, 112 pp.

Gardner, J.N., Reneau, S.L., Lewis, C.J., Lavine, A., Krier, D., WoldeGabriel, G., and Guthrie, G., 2001, "Geology of the Pajarito Fault Zone in the Vicinity of S-Site (TA-16), Los Alamos National Laboratory, Rio Grande Rift, New Mexico," Los Alamos National Laboratory Report LA-13831-MS, 86 pp.

Gardner, J.N., Reneau, S.L., Lavine, A., Lewis, C.J., Katzman, D., McDonald, E.V., Lepper, K., Kelson, K.I., and Wilson, C., 2003, "Paleoseismic Trenching in the Guaje Mountain Fault Zone, Pajarito Fault System, Rio Grande Rift, New Mexico," Los Alamos National Laboratory Report LA-14087-MS, 68 pp.

Gardner, J.N., Schultz-Fellenz, E.S., Caporuscio, F.A., Lewis, C.J., Kelley, R.E., and Greene, M.K., 2008, "Geology and Structure of the Chemistry and Metallurgy Research Facility Replacement Site, Los Alamos National Laboratory, New Mexico," Los Alamos National Laboratory Report LA-14378, 295 pp.

Goff, F., Gardner, J.N., and Reneau, S.L., 2001, "Geologic Map and Structure of the Frijoles Quadrangle, Los Alamos and Sandoval Counties, New Mexico," New Mexico Bureau of Geology and Mineral Resources, Geologic Open-File Map OF-GM 42, Scale 1:24,000.

Griggs, R.L., 1964, "Geology and Groundwater Resources of the Los Alamos Area, New Mexico," U.S. Geological Survey Water-Supply Paper 1753, 106 pp.

Hoek, E., Marinos, P., and Benissi, M., 1998, "Applicability of the Geological Strength Index (GSI) Classification for Very Weak and Sheared Rock Masses: The case of the Athens Schist Formation," *Bulletin of Engineering Geology and the Environment*, Vol. 57, pp. 151–160.

Izett, G.A. and J.D. Obradovich, 1994, "$^{40}Ar/^{39}Ar$ Age Constraints for the Jaramillo Normal Subchron and the Matuyama-Brunhes Geomagnetic Boundary," *Journal of Geophysical Research*, Vol. 99, pp. 2925–2934.

Jahn, A., 1964, "Slopes Morphological Features Resulting from Gravitation," *Zeitschrift fur Geomorphologie*, Supplement Band 5, pp. 59–72.

Jibson, R.W., 1993, "Predicting Earthquake-Induced Landslide Displacements Using Newmark's Sliding Block Analysis," *Transportation Research Record*, Vol. 1411, pp. 9–17.

- Jibson, R.W., and Keefer, D.K., 1993, "Analysis of Seismic Origin of Landslides: Examples from the New Madrid Seismic Zone," *Geological Society of America Bulletin*, Vol. 105, pp. 521–536.

- Krueger, J.W., 1992, RFI Work Plan for Operable Unit 1148, Environmental Restoration Program, Los Alamos National Laboratory Report LA-UR-92-855, Los Alamos, New Mexico.

Lavine, A., Lewis, C.J., Katcher, D.K., and Wilson, J., 2003, "Geology of the North-Central to Northeastern Portion of Los Alamos National Laboratory, New Mexico," Los Alamos National Laboratory Report LA-14043-MS, 44 pp.

Lewis, C.J., Gardner, J.N., Schultz-Fellenz, E.S., Lavine, A., Reneau, S.L., and Olig, S., 2009, "Fault Interaction and Along-Strike Variation in Throw in the Pajarito Fault System, North-Central

McCalpin, J.P., 2005. "Late Quaternary Activity of the Pajarito Fault, Rio Grande Rift of Northern New Mexico, USA," *Tectonophysics,* Vol. 408, pp. 213–236.

McCarroll, D., 1989, Potential and Limitations of the Schmidt Hammer for Relative-Age Dating: Field Tests on Neoglacial Moraines, Jotunheimen, Southern Norway," *Arctic and Alpine Research*, Vol. 21, No. 3, pp. 268–275.

McCarroll, D., 1991, "The Schmidt Hammer, Weathering, and Rock Surface Roughness," *Earth Surface Processes and Landforms*, Vol. 16, pp. 477–480.

Newmark, N.M., 1965, "Effects of Earthquakes on Dams and Embankments," *Geotechnique*, V. 15, pp. 139–159.

Phillips, E.H., Goff, F., Kyle, P.R., McIntosh, W.C., Dunbar, N.W., and Gardner, J.N., 2007, The $^{40}Ar/^{39}Ar$ Age Constraints on the Duration of Resurgence at the Valles Caldera, New Mexico," *Journal of Geophysical Research,* Vol. 112, DOI: 10.1029/2006JB004511.

Poths, J., and Goff, F., 1990, "Using Cosmogenic Nuclides to Estimate Erosion Rates," EOS: Transactions of the American Geophysical Union, Vol. 71, No. 43, p. 1346.

Purtymun, W.D., and Kennedy, W.R., 1971, "Geology and Hydrology of Mesita del Buey," Los Alamos National Laboratory Report LA-4660, 12 pp.

Quane, S.L., and Russell, J.K., 2005, "Ranking Welding Intensity in Pyroclastic Deposits," *Bulletin of Volcanology*, Vol. 67, pp. 129–143.

Rahman, M.D.H., and Khan, Y.A., 1995, "Landslides and Slope Stability of Coastal Cliffs of Cox's Bazar Area, Bangledesh," *Natural Hazards*, Vol. 12, pp. 101–118.

Reneau, S.L., 1995, "Potential Mesa-Edge Instability at Pajarito Mesa," *in* Reneau, S.L., and Raymond, R., Jr., eds., *Geological Site Characterization for the Proposed Mixed Waste Disposal Facility, Los Alamos National Laboratory*, Los Alamos National Laboratory Report LA-13089-MS, Los Alamos, New Mexico, pp. 87–100.

Reneau, S.L., Broxton, D.E., Carney, J.S., and LaDelfe, C., 1998, "Structure of the Tshirege Member of the Bandelier Tuff at Mesita del Buey, Technical Area 54, Los Alamos National Laboratory," Los Alamos National Laboratory Report LA-13538-MS, 21 pp.

Rogers, M.A., 1977, "History and Environmental Setting of LASL Near-Surface Land Disposal Facilities for Radioactive Wastes (Areas A, B, C, D, E, F, G, and T)," Los Alamos National Laboratory Report LA-6848-MS, Vol. 1, 266 pp.

Rogers, M.A., 1977, "History and Environmental Setting of LASL Near-Surface Land Disposal Facilities for Radioactive Wastes (Areas A, B, C, D, E, F, G, and T)," Los Alamos National Laboratory Report LA-6848-MS, Vol. 2, 168 pp.

Schaetzl, R., and Anderson, S., 2005, *Soils: Genesis and Geomorphology*, Cambridge University Press, 832 pp.

Schultz-Fellenz, E.S., and Kelley, R.E., 2009, "Evaluation of Potential Seismic Hazards from Holocene-age Surface-Rupturing Faults at Dome 375, Technical Area 54, Los Alamos National Laboratory," Los Alamos National Laboratory memorandum EES16-SHG-2009-001-R1, 10 pp.

Schultz-Fellenz, E.S., Coppersmith, R.T., Sussman, A.J., Swanson, E.M., Cooley, J.A., "Detecting Surface Changes from an Underground Explosion in Granite Using Unmanned Aerial System Photogrammetry," *Pure and Applied Geophysics*, 19 pp.

Schultz-Fellenz, E.S., Gardner, J.N., Lewis, C.J., Lavine, A., Reneau, S.L., in prep, "Re-evaluation of Holocene Paleoseismic Event Chronology in the Pajarito Fault System, Rio Grande Rift, Northern New Mexico," submitted to *Journal of Structural Geology*, 24 pp.

Seaward, M.R.D., Giacobini, C., Giuliani, M.R., Roccardi, A., 1989, "The Role of Lichens in the Biodeterioration of Ancient Monuments with Particular Reference to Central Italy, *International Biodeterioration*, Vol. 25, pp. 49–55.

Stirling, M., Ledgerwood, J., Liu, Tanzhuo, and Apted, M., 2010, "Age of Unstable Bedrock Landforms Southwest of Yucca Mountain, Nevada, and Implications for Past Ground Motion," *Bulletin of the Seismological Society of America*, Vol. 100, No. 1, pp. 74–86.

Wheaton, J.M., Brasington, J., Darby, S.E., and Sear, D.A., 2010, "Accounting for Uncertainty in DEMs from Repeat Topographic Surveys: Improved Sediment Budgets," *Earth Surface Processes and Landforms*, Vol. 35, No. 2, pp. 136-156.

Wilson, R.C., and Keefer, D.K., 1985, "Predicting Areal Limits of Earthquake-Induced Landsliding, *in* Ziony, J.I., ed., *Evaluating Earthquake Hazards in the Los Angeles Region: An Earth-Science Perspective*, U.S Geological Society Professional Paper 1360, pp. 316–345.

Wohletz, K.H., 1996, "Fracture Characterization of the Bandelier Tuff in OU-1098 (TA-2 and TA-41)," Los Alamos National Laboratory Report LA-13194-MS, 19 pp.

Wong, I., Kelson, K., Olig, S., Kolbe, T., Hemphill-Haley, M., Bott, J., Green, R., Kanakari, H., Sawyer, J., Silva, W., Stark, C., Haraden, C., Fenton, C., Unruh, J., Gardner, J., Reneau, S., and House, L., 1995, "Seismic Hazard Evaluation of the Los Alamos National Laboratory," Unpublished final report prepared for the Los Alamos National Laboratory and the U.S. Department of Energy, 3 Vols.

Wong, I., Silva, W., Olig, S., Dober, M., Gregor, N., Gardner, J., Lewis, C., Terra, F., Zachariasan, J., Stokoe, K., Thomas, P., and Upadhyaya, Shobhna, 2007, "Update of the Probabilistic Seismic Hazard Analysis and Development of Seismic Design Ground Motions at the Los Alamos National Laboratory," Unpublished final report prepared for the Los Alamos National Laboratory and the U.S. Department of Energy, 3 Vols.